CHEMMEDCHEM

CHEMISTRY ENABLING DRUG DISCOVERY

Accepted Article

Title: Phenotypic Prioritization of Diphyllin Derivatives that Block Filoviral Cell Entry by Vacuolar (H+)-ATPase Inhibition

Authors: Aaron R Lindstrom, Manu Anantpadma, Logan Baker, N. M. Raghavendra, Robert Davey, and Vincent Jo Davisson

To be cited as: *ChemMedChem* 10.1002/cmdc.201800587

Link to VoR: http://dx.doi.org/10.1002/cmdc.201800587

A Journal of

ChemPubSoc Europe

WILEY-VCH

www.chemmedchem.org

WILEY-VCH

FULL PAPER

Phenotypic Prioritization of Diphyllin Derivatives that Block Filoviral Cell Entry by Vacuolar (H^+)-ATPase Inhibition

Aaron Lindstrom[1], Manu Anantpadma[2], Logan Baker[1], N.M. Raghavendra[1-ff], Robert Davey[2], Vincent Jo Davisson*[1]

[1] Dr. A. Lindstrom, Mr. L. Baker, Dr. N.M. Raghavendra, Prof. V. J. Davisson
Department of Medicinal Chemistry and Molecular Pharmacology, College of Pharmacy
Purdue University
West Lafayette, IN 47907 USA
E-mail: davisson@purdue.edu

[2] Dr. M. Anantpadma, Prof. R. Davey
Department of Virology and Immunology
Texas Biomedical Research Institute
San Antonio, Texas, USA

Supporting information for this article is given via a link at the end of the document.

Abstract: Many viruses utilize endosomal pathways to gain entry to cells and propagate infection. Sensing of endosomal acidification is a trigger for release of many virus cores into the cell cytosol. Previous efforts with inhibitors of vacuolar-ATPase have been shown to block endosomal acidification and affect viral entry albeit with limited potential for therapeutic selectivity. Herein, four novel series of derivatives of the vacuolar-ATPase inhibitor diphyllin were synthesized to assess their potential for enhancing potency and anti-filoviral activity over cytotoxicity. Derivatives that suitably blocked cellular entry of Ebola pseudo-typed virus were further evaluated as inhibitors of endosomal acidification and isolated human Vacuolar-ATPase activity. Several compounds with significant increases in potency over diphyllin in these assays also separated from cytotoxic doses in human cell models by >100 fold. Finally, three derivatives were shown to be inhibitors of replication-competent Ebola viral entry into primary macrophages with comparable potencies and enhanced selectivity toward anti-viral activity.

Introduction

Filoviruses are highly contagious, lethal viruses that cause severe hemorrhagic fever in humans and primates.[1–3] They are negative-strand RNA, filamentous viruses that group into 3 families named Ceuvavirus, Ebolaviruses (EBOV) and Marburgviruses (MARV). Viruses from the latter two families are responsible for outbreaks that have up to 90% fatality, including the recent outbreak in West Africa that resulted in over 28,000 reported cases and 11,317 deaths.[4] Efforts are underway to develop novel EBOV therapies, including discovery of small molecule inhibitors,[5–10] repurposed drugs,[11–16] and vaccines.[17–20] Currently, there are no approved therapeutic measures for the treatment of filovirus infections but the development of a vaccine is being prioritized by the FDA and a promising viral polymerase inhibitor has also recently advanced in development.[21]

Filoviruses, like many other viruses, utilize the acidification of endosomes during their maturation to facilitate cellular entry.[22–25] Many cellular infections begin when individual virions are taken into cells by one of several mechanisms of endocytosis. As the virion-containing endosomes mature toward lysosomes, the luminal pH of the endosome decreases. EBOV requires this acidification to trigger penetration of the endosomal membrane by the filoviral glycoprotein to release the virus capsid into the cytosol and initiate replication. For enveloped viruses, penetration involves fusion of the virion's membrane with that of the endosome. Additionally, for filoviruses, pH-dependent endosomal proteases need to cleave the membrane glycoprotein into a fusion-capable form that interacts with the endosomal receptor NPC1.[26] Inhibitors of endosomal acidification are therefore potentially anti-filoviral and broad-spectrum anti-viral compounds.

A primary host factor responsible for endosomal acidification is the multi-subunit enzyme vacuolar (H^+)-ATPase (V-ATPase), whose role is to couple proton transport across cellular membranes with the hydrolysis of ATP.[27] In addition to endosomal acidification, many cellular and physiological processes are associated with V-ATPase function, including roles in renal pH homeostasis, osteoclast bone remodeling, and sperm maturation.[27–29] Different forms of V-ATPase are present in renal, neuronal, osteoclast and cancer cells along with the V-ATPase found in the endosomal membranes.[30] Dysregulation of specific isoforms have been associated with diseases, including osteoporosis, metastatic cancers, male infertility and renal acidosis.[31] Disease indications such as Ebola infection where treatment for acute conditions could justify the pursuit of V-ATPase inhibition. This case would be valid if useful therapeutic selectivity can be exhibited through structural modifications of the inhibitor chemotype.

Many natural product inhibitors of V-ATPase have been identified with a majority being macrocyclic lactones. Most of these natural inhibitors, such as bafilomycin A1 (Baf), have historic utility as cellular probes but lack the needed therapeutic selectivity to serve as drug leads due to off-target effects.[32,33] Diphyllin is an arylnaphthalene lignan and represents the only known phenylpropanoid-derived V-ATPase inhibitor to date.[34]

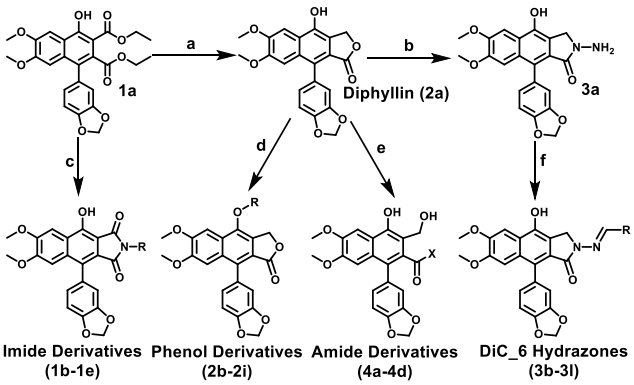

Scheme 1. **Synthesis of Diphyllin Derivatives.** Reagents and Conditions. (a) $LiAlH_4$, THF, 0°C, 1h (92%); (b) H_2NNH_2, MeOH, reflux, 12h (66%); (c) RNH_2, MeOH, reflux, 2-12h (57-93%); (d) RX, K_2CO_3, DMSO, 60°C, 1-48h (36-91%); (e) R_2NH, 0.5 M NaOH in MeOH, reflux, 12-18h (16-57%); (f) R_3CHO, MeOH, reflux, 6-12h (47-88%).

Cellular activities established for diphyllin have shown useful anti-tumor and antiosteoclastic activity,[34,35] as well as anti-viral activity in early testing using influenza and Dengue virus models.[36,37] The inhibition of pH-dependent virus infection and lack of cytotoxicity in tested cell lines prompted a feasibility study of diphyllin as a scaffold for a medicinal chemistry approach to develop selective V-ATPase inhibitors as potential broad-spectrum anti-viral agents. Two major questions about the diphyllin scaffold are addressed in this initial structure-activity work: a) if the biochemical and endosomal pH inhibition can be predictive of filoviral entry inhibition, and b) is there potential for enhancing V-ATPase inhibition without increasing risks of cytotoxicity?

There are advantages and disadvantages to host-specific anti-viral agents and an initial challenge is to establish therapeutic selectivity.[22] Herein, we report the identification of several novel diphyllin derivatives that are potent inhibitors of V-ATPase and EBOV infection of macrophages by phenotypic screening of a small library of diphyllin derivatives. The compounds were screened as inhibitors of EBOV pseudotype virus entry and endosomal acidification. Compounds selected from these screens were ranked by their potency against EBOV entry and dose selectivity of cellular endosomal acidification versus cytotoxicity. The positive hits were further assayed for the ability to inhibit V-ATPase activities in isolated vesicles. Three compounds were then evaluated on their ability to inhibit MARV cellular entry and replication-competent EBOV infection of primary human macrophages (PHMs) due to their importance as a site of filovirus infection.[38] Overall, this approach demonstrates the use of phenotypic screening to identify more selective V-ATPase inhibitors that block filoviral infection with reduced cytotoxicity.

Results and Discussion

Four series of diphyllin-related compounds were synthesized to determine the tolerance of modifications of the lactone ring and alkylation of the phenol functional group (**Scheme 1**). Synthesis of intermediate **1a** was completed using modified procedures

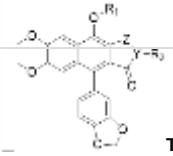

Table 1. Activity of diphyllin and derivatives against EBOV infection, endosomal acidification and cytotoxicity

ID	R_1	R_2	Y	Z	Pseudo-EBOV IC_{50} (nM)[a]	EA IC_{50} (nM)[b]	EA IC_{50}/CC_{50}[c]
Baf	-	-	-	-	14.9±8.93	40.5±3.31	7.90
1e			N	CO	5400±2920	>10000	ND
2a	H	-	O	CH_2	847±125	476±60.1	37.4
2b		-	O	CH_2	171±40.2	265±58.6	21.6
2c		-	O	CH_2	112±14.7	254±49.0	9.37
2d		-	O	CH_2	175±21.7	263±46.6	7.76
2e	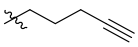	-	O	CH_2	73.2±11.9	102±19.0	39.6
2f	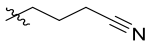	-	O	CH_2	93.1±26.8	98.7±29.5	31.7
2g	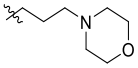	-	O	CH_2	107±23.7	74.3±23.9	151
2h	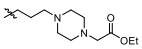	-	O	CH_2	132±32.3	172±40.6	144
2i	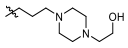	-	O	CH_2	76.2±14.6	104±21.2	299
3a	H		N	CH_2	3940±604	9060±893	5.40
3b	H	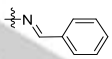	N	CH_2	6630±437	>10000	ND
3c	H	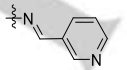	N	CH_2	4480±467	8710±769	5.73
3d	H	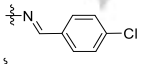	N	CH_2	1170±518	9930±140	2.86
3g	H	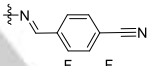	N	CH_2	1690±233	>10000	ND
3h	H	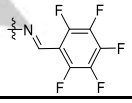	N	CH_2	8740±2180	>10000	ND

[a] Inhibition of GFP-expressing EBOV GP pseudotyped vesicular stomatitis virus (VSV) infection of HeLa cells; mean±SEM (n=6). [b] Inhibition of cellular endosomal acidification in HEK-293 cells; mean±SEM (n=9). [c] Selectivity Index of cytotoxicity (**Supplementary Table S2**) over endosomal acidification in HEK-293 cells.

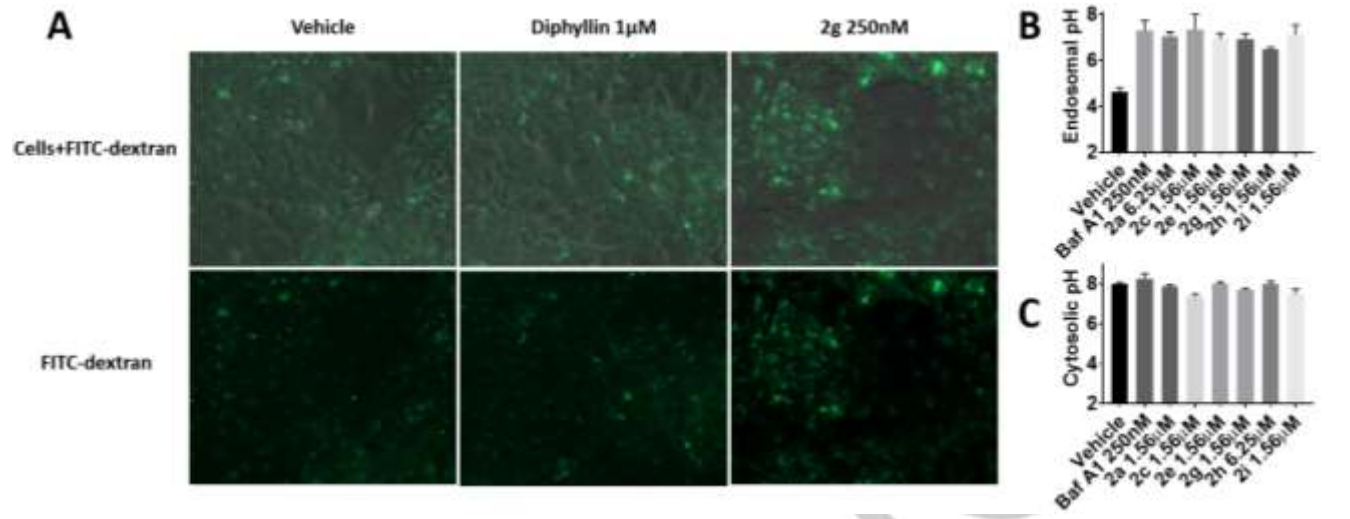

Figure 1. Diphyllin derivatives cause an increase in intracellular vesicle pH but no corresponding change in cytosolic pH. A) FITC-dextran stained (0.5mg/ml) HEK-293 cells after 4h treatment with chosen inhibitor or vehicle. B) Endosomal pH measured by FITC-dextran staining of HEK-293 cells after 4h treatment with chosen inhibitor or vehicle. C) Cytosolic pH measured by BCECF-AM staining (10μg/ml) of HEK-293 cells after 4h treatment with chosen inhibitor or vehicle.

from Charlton et al.[39] A set of imide derivatives were synthesized by condensation of primary amines with **1a** (Scheme 1). Diphyllin (**2a**) was synthesized from **1a** by selective reduction with lithium aluminum hydride and the final three series were synthesized with **2a** as the starting material. A set of propyl ether derivatives were synthesized by Williamson synthesis to incorporate tertiary amine and hydrophobic groups. The hydrazone derivatives were synthesized by first using the nucleophilic attack of hydrazine upon the lactone ring to create the hydrazide derivative **3a**. Then, condensation of **3a** with a set of substituted benzyl aldehydes provided a hydrazone series. Benzyl aldehydes were chosen with a broad range of physical properties, including pentafluoro, to test the toleration of modifications at the aryl position. Ring-opened amides were synthesized by nucleophilic attack of both primary and secondary amines upon the lactone ring of diphyllin to yield 1 secondary amide and 4 tertiary amides. All four classes were evaluated for potential PAINS alerts using SwissADME (**Supplementary Table S2**).[40] Only the hydrazone class demonstrate potential alerts, due to the imine functional group. All four classes were screened for the ability to inhibit EBOV infection using a GFP-expressing EBOV GP pseudotyped vesicular stomatitis virus (VSV) in HeLa cells (**Supplementary Fig. S1**). Diphyllin, one imide (**1e**), diphyllin hydrazide (**3a**), 5 hydrazones (**3b**-**d**, **g**, **h**), and all phenol ethers (**2b**-**i**) significantly inhibited the pseudotyped viral infection at 12.5 μM. Compounds were then ranked by IC_{50} to further evaluate the actives. Phenol ether derivatives demonstrated the greatest potency amongst those tested and **2e** displayed a 11.5-fold improvement in potency compared to diphyllin (**Table 1**). In general, phenol ether derivatives were the best class of derivatives with both hydrophobic and amino-alkyl ethers exhibiting improved potency compared to diphyllin. Hydrazones with para-substituted benzyl groups had the best activity within their class, though they were 1.4-fold less potent than diphyllin at best.

To evaluate a role for V-ATPase function as a mechanism for inhibition of EBOV cell entry, all active compounds were screened for the ability to inhibit endosomal acidification in HEK-293 cells. The dichromic dye acridine orange (AO) freely passes through cells in its uncharged form but accumulates in acidic endosomal compartments as the dye becomes protonated and aggregates. The ratio between the neutral dye, which emits at 530 nm, and the charged dye, which shifts its emission to 650 nm, can be used to detect vesicle acidification in cells.[37,41] Candidate V-ATPase inhibitors were identified in HEK-293 cells by a significant decrease in the 650 nm/530 nm ratio of AO fluorescence when compared to the vehicle control. The IC_{50} values for inhibition of endosomal acidification (EA assay) where then compared with the cytotoxicity values (CC_{50}) in the same cell lines to determine if the different activities could be separated. In this assay, known V-ATPase inhibitors Baf and diphyllin (**2a**) showed a potency that was consistent with those observed in the pseudo-EBOV cell entry. The well-established V-ATPase inhibitor Baf was more potent than diphyllin in the assay but its cytotoxicity was also significantly enhanced. Activity was tested in two cell lines (HEK-293 and A549) to assess the activity of derivatives in different cell environments. The A549 cell line was chosen for comparison to previous reports using diphyllin, while HEK-293 cells offer a model relevant to previous EBOV inhibitor screens.[8,37,42,43]

Table 2. Inhibitory Activity of Derivatives against Isolated Human V-ATPase

ID	Proton Pump IC_{50} (nM)[a]	ATPase Inhibition[b]
Baf	24.8±2.66	(+)
2a	189±1.66	(+)
3c	423±3.96	(-)
3d	724±13.5	(-)
2b	47.5±5.28	(+)
2c	16.9±3.72	(+)
2e	11.7±2.97	(+)
2g	27.4±3.88	(+)
2h	114±1.71	(+)
2i	61.0±2.84	(+)

(+) denotes significantly less Pi released than control ($p>0.01$). [a] Inhibition of V-ATPase induced AO quenching; mean±SEM (n=9). [b] Inhibition of V-ATPase induced ATP hydrolysis; mean±SEM (n=9).

The endosome acidification screen identified significant differences among the three diphyllin analog classes selected from the original screen (**Table 1** and **Supplementary Fig. S2**). Overall, the relative potencies in this assay track with the EBOV cell entry effects. Imide **1e** did not cause a significant change in the fluorescence ratio, indicating a lack of any effect on endosomal acidification. Hydrazide **3a** and four of the six active hydrazones moderately inhibited acidification but none achieved the level of inhibition observed with **2a**. Only hydrazide **3a** and hydrazones **3c** and **3d** inhibited acidification to the level observed with Baf at concentrations higher than 10 μM but these compounds were 18-fold less potent than diphyllin on average (**Supplementary Fig. S3**). Unfortunately, the cytotoxicity of this class of compounds had minimal separation from inhibition of endosomal acidification. The 10-fold difference between IC_{50} values in the two assays for this class likely indicate activity against a separate target during EBOV entry assay.

The phenol derivatives presented a different profile from the other classes when endosomal acidification and cytotoxicity were assessed (**Table 1** and **Supplementary Fig. S3**). All phenol ethers inhibited acidification at a level similar to Baf and exhibited improved IC_{50} values compared with diphyllin. Remarkably, the basic heterocycle containing derivatives (**2g**-**2i**) also exhibited up to an 8-fold improvement in separation of cytotoxicity compared with diphyllin (38-fold compared to Baf) in HEK-293 cells as indicated by the IC_{50}/CC_{50} ratios. These derivatives potently inhibited endosomal acidification and exhibited decreased cytotoxicity compared to diphyllin in both HEK-293 and A549 cell lines. The morpholino ether derivative **2g** was the more potent derivative in both cell lines and demonstrated similar cytotoxicity to diphyllin. The piperazinyl acetate ether **2h** demonstrated less activity compared to the morpholino but also had lower cytotoxicity and a similar separation as **2g** in HEK-293 cells. Derivative **2i** demonstrated the greatest separation of the ether derivatives at nearly 300. Interestingly, the lipophilic derivatives exhibited a similar, or better, potency compared to the amino ethers but also increases in cell toxicity. Derivative **2f** had a similar potency to **2g** in the endosomal acidification assay but increased cytotoxicity 5-fold relative to diphyllin. Alkyl derivative **2c** was the most potent of all derivatives in the A549 cell line but 4-fold less potent in HEK-293 cells (**Supplementary Table S1**) and more cytotoxic. Thus, while the lipophilic derivatives demonstrated greater potency than diphyllin, they were more cytotoxicity up to 10-fold in HEK-293 cells. Overall, far less cytotoxicity was observed in A549 cells for all tested ethers compared to HEK-293 cells but activities against endosomal acidification were similar. In general, the more basic derivatives expanded the separation of endosomal acidification and cytotoxicity in HEK-293 cells compared to diphyllin. The lack of discrimination of cytotoxicity observed with the A549 cells indicate their utility to be minimal since they lack the level of stringency needed to define therapeutically selective inhibitors.

Since acridine orange is a promiscuous dye and can integrate with nucleic acids to also give a fluorescent emission, FITC-dextran fluorescence was used to further assess the ability of our top compounds to change endosomal pH. FITC-dextran is exclusively trapped in endosomes and the FITC fluorescence is quenched by increasing acidity. Fluorescent microscopy of FITC-dextran stained cells indicated that diphyllin and amino ether **2g** demonstrated increased FITC fluorescence relative to the vehicle-treated control (**Fig. 1A**). FITC-dextran was also used to quantify endosomal pH in cells treated with diphyllin and derivatives.

Both diphyllin and all tested derivatives resulted in elevated endosomal pH (pH 7) at low micromolar concentrations (1-7 μM; **Fig. 1b**). To ensure that the change in endosomal pH was not due to an overall change in cellular pH, cytosolic pH was measured with the BCECF-AM dye mixture. Treatment with Baf**, 2a** and its derivatives showed no significant change in cytosolic pH compared to the vehicle treated control (**Fig. 1C**). In combination with the acridine orange assays, these results are consistent with no optical interference by the arylnaphthalene lactone chromophore.

To assess if the inhibition of endosomal acidification results from a block in V-ATPase activity, the active diphyllin derivatives were tested in the proton-pumping and ATPase functional assays. Vesicles containing V-ATPase were isolated from HEK-293 cells by adapting a published method.[44] To determine the effect of compounds upon the proton-pumping function of V-ATPase, vesicles were pre-incubated with acridine orange and the test compound or vehicle for 1 h prior to the addition of ATP to initiate pump activity. Quenching of the 530 nm emission of acridine orange was measured over 1 h before addition of nigericin to relax the proton gradient within vesicles. IC_{50} values for hit compounds from the cellular assays were calculated by measuring the change in AO fluorescence immediately before and after the addition of nigericin **(Supplementary Fig. S4).** Overall, inhibition of V-ATPase activities followed a similar activity profile to the cellular assays. Diphyllin was 7.5 times less potent than Baf at inhibiting V-ATPase-mediated fluorescent quenching (**Table 2**). All phenol derivatives had improved inhibitory potency relative to diphyllin and several had similar activities to Baf. The lipophilic and amino phenol derivatives had 8-17 times greater potencies relative to diphyllin with 2e demonstrating a 2-fold improvement over Baf. Hydrazone derivatives **3c** and **3d** were 2 and 4 times less potent, respectively, than diphyllin which provided additional evidence that these are weak inhibitors of V-ATPase and less selective for the on-target effects.

Using the same vesicle preparations, the effect of the diphyllin derivatives on ATP hydrolysis by V-ATPase was evaluated. Isolated HEK-293 vesicles were pre-incubated with the active compounds for 1 h at a concentration of 1 μM. ATP was then Using the same vesicle preparations, the effect of the diphyllin derivatives on ATP hydrolysis by V-ATPase was evaluated.

Table 3. Anti-Filoviral activity of Diphyllin and Top Derivatives in HeLa and Primary Human Macrophages

ID	HeLa CC_{50} (μM)[a]	Pseudo-EBOV IC_{50}/CC_{50}[b]	Pseudo-MARV IC_{50} (nM) [c]	MARV IC_{50}/CC_{50}[b]	PHM EBOV IC_{50} (nM)[d[	PHM IC_{50}/CC_{50}[b]
2a	>100	>147	1770±80.0	>56.5	678±218	>73.7
2e	36.5±7.13	499	402±45.9	90.8	240±36.4	>416
2g	36.6±18.8	342	135±11.4	271	57.7±8.6	>1530
2h	63.0±11.2	477	81.6±28.7	772	256±21.3	>391

[a] Cellular cytotoxicity for select compounds; mean±SEM (n=6). [b] Selectivity index between cytotoxicity and inhibition of infection. [c] Inhibition of GFP-expressing MARV GP pseudotyped vesicular stomatitis virus (VSV) infection of HeLa cell; mean±SEM (n=6). [d] Inhibition of replication-competent EBOV infection; mean±SEM (n=6).

Using the same vesicle preparations, the effect of the diphyllin derivatives on ATP hydrolysis by V-ATPase was evaluated. Isolated HEK-293 vesicles were pre-incubated with the active compounds for 1 h at a concentration of 1 µM. ATP was then added to the vesicles and the amount of ATP hydrolyzed after 1 h was measured using malachite green to quantify free phosphate released by ATPase action. Diphyllin and the phenol ether derivatives inhibited ATP hydrolysis to a similar extent at 1 µM compared to Baf, while hydrazones **3c** and **3d** did not (**Table 2** and **Supplementary Fig. S5**). These data are consistent with the cellular endosomal assay screen and verify that the work-flow identifies compound as significant V-ATPase inhibitors that block viral cellular entry.

To further substantiate the compound effects in these assays, diphyllin and compounds **2e** and **2g** were all evaluated for time dependence of effects in both the cellular endosomal acidification assay and the biochemical assay (**Supplementary Fig. S6, S7**). In both cases, there was no observed time dependent changes in the percent inhibition. The chemical stability of compounds **2a**, **2f**, **2g**, **2i**, **3d** were also evaluated in cell culture media. In the time course of the inhibition assays, no significant degradation products were observed (**Supplementary Fig. S8**). Compounds **2a, 2f, 2g** were also tested for stability in HEK-293 cell culture for 24 h (**Supplementary Fig. S9**) and no apparent degradation products were observed. Finally, UV-vis spectra were obtained of both **2a** and **2g** to ensure there was no overlap of the diphyllin chromophore with the excitation/emission spectra of the dyes used (**Supplementary Fig. S10**). There was little fluorescence beyond the 400nm and no overlap with the fluorophores leading to the conclusion that there was no interference with the fluorophores used. Therefore, the activity observed for the top inhibitors is against V-ATPase via non-covalent actions.

To determine if our derivatives are broadly active against filoviruses, the top active derivatives were tested for the ability to inhibit MARV infection. While related to EBOV, MARV utilizes different cellular entry pathways from EBOV but it is still dependent upon endosomal acidification.[45] Therefore, the top active amino and hydrophobic phenol ether derivatives, **2e**, **2g**, and **2h** were further assessed for activity against MARV cellular entry in the HeLa cell model using a GFP-expressing MARV GP-pseudotyped VSV. Both derivative **2e** and diphyllin suffered significant losses in potency against MARV compared with their activities against EBOV infection. However, amino ether derivatives **2g** and **2h** did not significantly change potency against MARV compared with their activities against EBOV infection, indicating these derivatives may have a broader anti-viral activity (**Table 3**). These data indicate that the derivatives, especially the amino-alkyl derivatives, selectively block activities required for cell entry common to both classes of filoviruses without increasing cytotoxicity (**Table 3**).

The top active derivatives were used to evaluate the inhibition of replication-competent EBOV infection of primary human macrophages with impressive results. Macrophages and other monocyte-derived cells are a primary cell target of infection by EBOV and derivative activity against EBOV infection in this model may better indicate activity during host infection. The three compounds tested in macrophage had a greater than 3-fold improvement in activity over diphyllin, with **2g** having the most potent activity (11.8-fold). The derivatives also displayed greater separations (>300X) of anti-viral activity over cytotoxicity in the primary macrophages. Note that the only compound with a measurable CC_{50} was **2g**, which had a separation of 1525 from IC_{50} which indicates an even greater separation for the other two derivatives. For instance, compound **2h** showed lower cytotoxicity than **2g**. Overall, these data indicate that these derivatives are potent inhibitors of EBOV infection of macrophages and appear safe within a wide range of active concentrations.

Conclusions

In summary, we synthesized four classes of diphyllin derivatives and tested them for the ability to inhibit EBOV infection and cellular endosomal acidification. Phenol ethers proved to be among the most potent V-ATPase inhibitors reported to date and this activity directly correlated with blockade of cellular endosomal acidification and EBOV infection. The activities of the derivatives against filovirus cell entry and endosomal acidification were paralleled by the activity against isolated V-ATPase containing vesicles. Together, these data are consistent with a mechanism of blocking viral infection that involves inhibition of V-ATPase. Concordantly, the less active V-ATPase inhibition of the hydrazone and imide classes show reduced potency and dose selectivity in cell-based assays.

The best derivatives herein described have very potent V-ATPase inhibitory activities but less cytotoxicity than compared to known V-ATPase inhibitors. The increase in selectivity for the alkylamine phenol derivatives may be due to trapping within the endosome. This localization would trap the compounds in acidic organelles by protonation of the amine functional group where the virus, V-ATPase, and inhibitor must co-localize. Confining the inhibitor to the organelles where V-ATPase is active could minimize off-target effects of the inhibitors within cells and thus minimize toxicity. Further studies of the alkylamine group could lead to optimization of the compounds selectivity and *in vivo* evaluation of potential metabolic liabilities of the scaffold is also needed. Overall, these results represent the first example of structural derivatization of a natural product scaffold to enhance the selectivity of V-ATPase inhibitors for blocking viral cell entry.

Experimental Section

Chemistry

General: All commercially purchased reagents used in this study were of the hghest purity available. Regular solvents (THF, ethyl acetate, dichloromethane, dimethyl sulfoxide, etc.) were used as recieved without further purification. NMR spectra were recorded at 298 K on Bruker ARX300, DRX500, and Avance-III-800 spectrometers using DMSO-d_6 as the solvent and internal reference (δ_H=2.46 ppm, δ_C=40.0 ppm). Chemical shifts are reported in parts per million (ppm) and coupling constants (*J*) are given in Hertz (Hz). The proton spectra are reported as follows δ (multiplicity, coupling constant, number of protons). Proton multiplicities are designated as follows: s(sin-glet), d(doublet), t(triplet), q(quartet), and m(multiplet). High resolution mass spectra were taken using an Agilent 6550 Q-Tof mass spectrometer using electrospray ionization (ESI). Low resolution mass spectra were taken on an Advion expression Compact Mass Spectrometer using ESI. High performance liquid chromatography (HPLC) was performed on a Hitachi D-7000 system using a Phenomenex Kromasil C18 column with water and acetonitrile (ACN) solvents containing 1% trifluoroacetic acid. HPLC was used for purity determination using a general method as follows: 5% ACN for 1 min, 5-100% ACN over 15min, 100% ACN for 2 min, 100-5% ACN for 2 min.

9-(benzo[d][1,3]dioxol-5-yl)-4-hydroxy-6,7-dimethoxynaphtho[2,3-c]furan-1(3H)-one (**2a**)- **1a** was synthesized using methods previously published in Charlton et al.[46] **1a** (511 mg, 1.05 mmol, 1 eq.) was dissolved in 20 mL of tetrahydrofuran (THF) and cooled to 0°C in an ice bath. This solution was added dropwise to a stirring solution of 50mL of lithium aluminum hydride (79.7mg, 2.10 mmol, 2 eq.) dissovled in THF. After 1h at 0°C, the reaction was quenched with saturated sodium sulfate, filtered through celite, and concentrated under reduced pressure. The crude mixture was extracted with ethyl acetate (3x50 mL) and washed with water (50 mL) and brine (50 mL). The water layers were combined and acidified with 1M HCl. The resulting precipitate was filtered to yield a yellow solid (368 mg, 92%, Purity: 97.5%). ^{1}H NMR (500 MHz, DMSO-d_6) δ 10.39 (s, 1H), 7.61 (s, 1H), 7.00 (d, *J* = 7.8 Hz, 1H), 6.94 (s, 1H), 6.85 (d, *J* = 1.6 Hz, 1H), 6.74 (dd, *J* = 7.9, 1.7 Hz, 1H), 6.10 (d, *J* = 1.3 Hz, 2H), 5.35 (s, 2H), 3.93 (s, 3H), 3.64 (s, 3H). ^{13}C NMR (126 MHz, DMSO-d_6) δ 170.0, 150.9, 150.0, 147.2, 146.9, 145.2, 129.8, 129.1, 124.1, 123.6, 122.0, 119.0, 111.4, 108.2, 105.7, 101.4, 101.0, 66.9, 56.3, 55.9, 55.4. ESI-MS (ESI+) *m/z*: calculated for $C_{21}H_{16}O_7$+H$^+$, 381.0969 [M+H]$^+$, found 381.0964 [M+H]$^+$.

2-amino-4-(benzo[d][1,3]dioxol-5-yl)-9-hydroxy-6,7-dimethoxy-1H-benzo[f]isoindole-1,3(2H)-dione (**1b**)- **1a** (148 mg, 0.316mmol) was dissolved in methanol (5 mL) and heated to reflux. Hydrazine hydrate (500ul, ~60% solution) was added dropwise and the reaction was refluxed overnight. Precipitate formed upon cooling the mixture to -20°C and was filtered off to yield a pure, yellow solid (121mg, 93%, Purity: 99.3%). ^{1}HNMR (500MHz, DMSO-d_6): 8.53 (s, 1H), 7.68 (s, 1H), 7.11 (s, 1H), 6.97 (d, *J*=10Hz, 1H), 6.86 (s, 1H), 6.85 (d, 1.5Hz, 1H), 6.09 (d, *J*=20Hz, 2H), 4.08 (s, 3H), 4.07 (s, 2H), 3.83 (s, 3H). LC-MS *m/z*: calculated for $C_{21}H_{16}N_2O_7$+H$^+$, 409.1 [M+H]$^+$, found 409.2 [M+H]$^+$.

4-(benzo[d][1,3]dioxol-5-yl)-9-hydroxy-2-(2-hydroxyethyl)-6,7-dimethoxy-1H-benzo[f]isoindole-1,3(2H)-dione (**1c**)- **1a** (150mg, 0.320mmol) was dissolved in methanol (5ml) and heated to reflux. Ethanolamine (1ml, 1.012g, 16.6mmol) was added dropwise and the reaction was allowed to react overnight. The reaction was cooled and methanol was removed by rotary evaporation. The remaining liquid was acidified by 1M HCl and the resulting precipitate was collected by vacuum filtration. The precipitate was recrystallized from toluene and methanol to yield 120mg (85%, Purity: 95.1%) of yellow solid. ^{1}HNMR (500MHz, DMSO- d_6): 7.78(s, 1H), 7.03 (s, 1H), 6.93 (d, *J*=10Hz, 1H), 6.82 (s, 1H), 6.80 (d, *J*=10Hz, 1H), 6.02 (d, *J*=5Hz, 2H), 4.59 (s, 2H), 3.97 (s, 3H), 3.72 (s, 3H), 3.68 (s, 4H). LC-MS *m/z*: calculated for $C_{23}H_{19}NO_8$+H$^+$, 438.1 [M+H]$^+$, found 438.1 [M+H]$^+$.

4-(benzo[d][1,3]dioxol-5-yl)-9-hydroxy-6,7-dimethoxy-2-(2-morpholinoethyl)-1H-benzo[f]isoindole-1,3(2H)-dione (**1d**)- **1a** (102mg, 0.218mmol) and was dissolved in methanol (5ml) and heated to reflux. 4-(2-aminoethyl)morpholine (1ml, 0.992g, 7.62mmol) was added dropwise and the reaction proceeded overnight. The reaction was cooled and methanol was concentrated under reduced pressure. The crude mixture was extracted with ethyl acetate (3x20ml) and the organic layers were combined and washed with distilled water (20mL) and brine (20mL). The organic layer was dried with anhydrous sodium sulfate and concentrated by under reduced pressure. The crude solid was recrystallized from toluene and methanol to yield an amorphous, yellow solid (61mg, 57%, Purity: 95.3%). ^{1}H NMR (500 MHz, DMSO-d_6) δ 10.96 (s, 1H), 9.56 (s, 1H), 7.74 (s, 1H), 7.04 – 6.97 (m, 2H), 6.90 (d, *J* = 1.7 Hz, 1H), 6.79 (dd, *J* = 7.9, 1.7 Hz, 1H), 6.09 (d, *J* = 7.5 Hz, 2H), 4.01 – 3.95 (m, 2H), 3.93 (s, 3H), 3.87 – 3.83 (m, 2H), 3.66 (s, 3H), 3.56 (d, *J* = 12.4 Hz, 4H), 3.10 (d, *J* = 11.0 Hz, 2H). LC-MS *m/z*: calculated for $C_{27}H_{26}N_2O_8$+H$^+$, 507.2 [M+H]$^+$, found 507.1 [M+H]$^+$.

9-(benzo[d][1,3]dioxol-5-yl)-2-(2-hydroxyethyl)-6,7-dimethoxy-1,3-dioxo-2,3-dihydro-1H-benzo[f]isoindol-4-yl acetate (**1e**)- Imide **1c** (110 mg, 0.252mmol), activated zinc dust (200 mg), and acetic acid (20mL) were added to a reaction flask and heated to reflux overnight. The reaction was cooled to room temperature and the precipitate was filtered off and the filtrate was washed with methanol until only a black precipitate remained. The filtrate was condensed under reduced pressure and the crude product was separated by silica gel column chromatography (hexanes: ethyl acetate 5:5 to 0:100) to yield a fluorescent, green solid (64 mg, 53%, Purity: 97.5%). ^{1}H NMR (500 MHz, DMSO-d_6) δ 7.70 (s, 1H), 7.03 – 6.93 (m, 2H), 6.90 (d, *J* = 1.7 Hz, 1H), 6.80 – 6.74 (m, 1H), 6.09 (d, *J* = 2.9 Hz, 2H), 4.14 (t, *J* = 5.5 Hz, 2H), 3.92 (s, 3H), 3.64 (s, 3H), 1.90 (s, 3H), 1.00 (s, 1H). ESI-MS (ESI+) *m/z*: calculated for $C_{25}H_{21}NO_9$+H$^+$, 480.1295 [M+H]$^+$, found 480.1289 [M+H]$^+$.

Synthesis of Hydrophobic Phenol Ethers: Gerenal Procedure. 2a (1eq), haloalkane (2eq), and potassium carbonate (5eq) were dissolved in dimethyl sulfoxide (6mL). The reaction was heated to reflux overnight. The reaction was then cooled to room temperature and 20mL of distilled water was added to the flask. The mixture was added to a separatory funnel and extracted with dichloromethane (3x20mL). The organic layers were combined and washed with distilled water (30mL) and brine (30mL) before concentrating the organic layers under reduced pressure. The crude product was purified with normal phase silica gel chromatography (Hexanes/EtOAc 100/0 to 80/100) to yield the pure solid.

9-(benzo[d][1,3]dioxol-5-yl)-4,6,7-trimethoxynaphtho[2,3-c]furan-1(3H)-one (**2b**)- **2a** (50mg, 0.131mmol, 1eq), methyl iodide (20µl, 22.8mg, 2.5eq), and potassium carbonate (91mg, 0.655mmol, 5eq) were dissolved in dimethyl sulfoxide (6mL). The reaction was heated to reflux overnight. The reaction was worked up and purified as above to yield a white solid (yield: 46mg, 91%, Purity: 98.0%). ^{1}H NMR (500 MHz, DMSO-d_6) δ 7.49 (s, 1H), 7.00 (d, *J* = 7.9 Hz, 1H), 6.92 (s, 1H), 6.84 (d, *J* = 1.6 Hz, 1H), 6.72 (dd, *J* = 7.9, 1.7 Hz, 1H), 6.09 (s, 2H), 5.69 (s, 2H), 4.11 (s, 3H), 3.92 (s, 3H), 3.62 (s, 3H). 13C NMR (201 MHz, DMSO-d_6) δ 169.5, 151.7, 150.4, 147.7, 147.4, 147.2, 133.0, 129.9, 128.9, 125.3, 124.2, 124.1, 119.47, 111.3, 108.4, 105.9, 101.6, 101.0, 67.2, 59.5, 56.1, 55.7, 21.2. ESI-MS (ESI+) *m/z*: calculated for $C_{22}H_{18}O_7$ +H$^+$, 395.1125 [M+H]$^+$, found 395.1125[M+H]$^+$.

9-(benzo[d][1,3]dioxol-5-yl)-4-ethoxy-6,7-dimethoxynaphtho[2,3-c]furan-1(3H)-one (**2c**)- **2a** (51mg, 0.134mmol, 1eq), ethyl bromide (20µl, 29.2mg, 2eq), and potassium carbonate (90mg, 0.651mmol, 5eq) were dissolved in dimethyl sulfoxide (6mL). The reaction was heated to reflux overnight. The reaction was worked up and purified as above to yield an off-white/yellow solid (yield: 40mg, 74%, Purity: 99.1%). ^{1}H NMR (500 MHz, DMSO-d_6) δ 7.48 (s, 1H), 6.99 (d, *J* = 7.9 Hz, 1H), 6.92 (s, 1H), 6.84 (d, *J* = 1.7 Hz, 1H), 6.72 (dd, *J* = 7.9, 1.7 Hz, 1H), 6.09 (s, 2H), 5.72 (s, 2H), 5.57 (s, 2H), 4.29 (q, *J* = 7.0 Hz, 2H), 3.91 (s, 3H), 3.62 (s, 3H), 1.42 (t, *J* = 7.0 Hz, 3H). ^{13}C NMR (201 MHz, DMSO-d_6) δ 169.5, 151.7, 150.4, 147.4, 147.2, 146.9, 133.3, 129.9, 128.9, 126.1, 125.8, 124.1, 119.4, 111.3, 108.4, 106.0, 101.5, 101.1, 68.0, 67.1, 56.0, 55.7, 31.1, 16.1. ESI-MS (ESI+) *m/z*: calculated for $C_{23}H_{20}O_7$ +H$^+$, 409.1281 [M+H]$^+$, found 409.1276 [M+H]$^+$.

9-(benzo[d][1,3]dioxol-5-yl)-6,7-dimethoxy-4-(prop-2-yn-1-yloxy)naphtho[2,3-c]furan-1(3H)-one (**2d**)- **2a** (50mg, 0.131mmol, 1eq), propargyl bromide (30µl of 80 wt.% solution in toluene, 2eq), and potassium carbonate (85mg, 0.615mmol, 5eq) were dissolved in dimethyl sulfoxide (6mL). The reaction was heated to reflux overnight. The reaction was worked up and purified as above to yield a light brown solid (yield: 31mg, 56%, Purity: 95.8%). ^{1}H NMR (500 MHz, DMSO-d_6) δ 7.52 (d, *J* = 1.9 Hz, 1H), 7.01 (dd, *J* = 7.9, 1.9 Hz, 1H), 6.95 (d, *J* = 1.9 Hz, 1H), 6.87 (d, *J* = 1.8 Hz, 1H), 6.74 (dd, *J* = 7.9, 1.8 Hz, 1H), 6.10 (d, *J* = 1.9 Hz, 2H), 5.59 (s, 2H), 5.00 (d, *J* = 2.4 Hz, 2H), 3.93 (s, 3H), 3.70 (t, *J* = 2.4 Hz, 1H), 3.63 (s, 3H). ^{13}C NMR (201 MHz, DMSO-d_6) δ 169.4, 151.8, 150.5, 147.4, 147.3, 146.0, 134.6, 130.1, 128.6, 127.6, 126.6, 124.0, 119.2, 111.3, 108.4, 106.0, 101.6, 101.2, 80.1, 79.8, 66.9, 60.4, 56.1, 55.7. ESI-MS (ESI+) *m/z*: calculated for $C_{24}H_{18}O_7$ +H$^+$, 419.1125 [M+H]$^+$, found 419.1129 [M+H]$^+$.

9-(benzo[d][1,3]dioxol-5-yl)-6,7-dimethoxy-4-(pent-4-yn-1-yloxy)naphtho[2,3-c]furan-1(3H)-one (**2e**)- **2a** (49mg, 0.129mmol, 1eq), 5-chloro-1-pentyne (28µl, 26.9mg, 2eq), and potassium carbonate (89mg, 0.644mmol, 5eq) were dissolved in dimethyl sulfoxide (6mL). The reaction was heated to reflux overnight. The reaction was worked up and purified as above to yield a white solid (yield: 36mg, 61%, Purity: 98%). ^{1}H NMR (500 MHz, DMSO-d_6) δ 7.48 (s, 1H), 7.02 – 6.91 (m, 2H), 6.85 (d, *J* = 1.6 Hz, 1H), 6.73 (dd, *J* = 7.8, 1.7 Hz, 1H), 6.09 (s, 2H), 5.56 (s, 2H), 4.28 (t, *J* = 5.9 Hz, 2H), 3.92 (s, 3H), 3.62 (s, 3H), 2.86 (t, *J* = 2.7 Hz, 1H), 2.50 – 2.48 (m, 2H), 2.00 (q, *J* = 6.5 Hz, 2H). ^{13}C NMR (126 MHz, DMSO-d_6) δ 169.4, 151.6, 150.3, 147.2, 147.1, 146.5, 133.5, 129.8, 128.6, 126.1, 126.0, 123.9, 119.3, 111.2, 108.3, 105.8, 101.4, 100.7, 84.0, 72.3, 70.6, 66.9, 55.9, 55.5, 28.9, 15.0. ESI-MS (ESI+) *m/z*: calculated for $C_{26}H_{22}O_7$ +H$^+$, 447.1438 [M+H]$^+$, found 447.1432 [M+H]$^+$.

4-((9-(benzo[d][1,3]dioxol-5-yl)-6,7-dimethoxy-1-oxo-1,3-dihydronaphtho[2,3-c]furan-4-yl)oxy)butanenitrile (**2f**)- **2a** (51mg, 0.134mmol, 1eq), 4-bromobutyronitrile (27µl, 38.8mg, 2eq), and potassium carbonate (89mg, 0.644mmol, 5eq) were dissolved in dimethyl sulfoxide (6mL). The reaction was heated to reflux overnight. The reaction was worked up and purified as above to yield a white solid (yield: 21mg, 36%, Purity: 95.1%. ^{1}H NMR (500 MHz, DMSO-d_6) δ 7.54 (s, 1H), 7.03 – 6.91 (m, 2H), 6.86 (d, *J* = 1.7 Hz, 1H), 6.73 (dd, *J* = 7.9, 1.7 Hz, 1H), 6.09 (s, 2H), 5.61 (s, 2H), 4.33 (t, *J* = 5.8 Hz, 2H), 3.94 (s, 3H), 3.63 (s, 3H), 2.80 (t, *J* = 7.0 Hz, 2H), 2.13 (q, *J* = 6.5 Hz, 2H). ^{13}C NMR (201 MHz, DMSO-d_6) δ 169.4, 151.8, 150.4, 147.4, 147.3, 146.5, 133.6, 130.0, 128.8, 125.8, 125.6, 124.0, 121.0, 119.4, 111.3, 108.4, 106.0, 101.5, 101.1, 70.6, 67.1, 56.2, 55.7, 26.0, 14.1. ESI-MS (ESI+) *m/z*: calculated for $C_{25}H_{21}NO_7$ +H$^+$, 448.1390 [M+H]$^+$, found 448.1287 [M+H]$^+$.

Synthesis of chloro-propylamine precursors: General Procedure. 1-bromo-3-chloropropane (1.1mL, 1.72g, 11mmol; 1.5eq) and amine component (1eq) were dissolved in acetonitrile (40mL) at room temperature while stirring. triethylamine (3.1 mL, 2.2g, 2eq) of was added dropwise and the reaction mixture was stirred at room temperature for 24-48 hours. When reaction was deemed complete by thin-layer chromatography, the solvent was removed under reduced pressure to yield a crude oil. The crude oil was purified by normal phase silica gel chromatography (DCM/MeOH 100/0 to 50/50) to yield the pure oil.

4-(3-chloropropyl)morpholine (**2ga**)- 1-bromo-3-chloropropane (1.1mL, 1.72g, 11mmol; 1.5eq) of 1-bromo-3-chloropropane and amine component (641µl, 639mg, 1eq) were dissolved in acetonitrile (40mL) at room temperature while stirring. triethylamine (3.1mL, 2.2g, 2eq) was then added dropwise, the reaction mixture was stirred at room temperature for 24h and purified as above to yield a yellow oil (yield: 351mg, 30%). LC-MS *m/z*: calculated for $C_7H_{14}ClNO$+H$^+$, 164.1 [M+H]$^+$, found 164.1 [M+H]$^+$.

Ethyl 2-(4-(3-chloropropyl)piperazin-1-yl)acetate (**2ha**)- 1-bromo-3-chloropropane (1.1mL, 1.72g, 11mmol; 1.5eq) of 1-bromo-3-chloropropane and amine component (1.16g, 1eq) were dissolved in acetonitrile (40mL) at room temperature while stirring. triethylamine (3.1mL, 2.2g, 2eq) was then added dropwise, the reaction mixture was stirred at room temperature for 24h and purified as above to yield a yellow oil (yield: 654mg, 36%). LC-MS *m/z*: calculated for $C_{11}H_{21}ClN_2O_2+H^+$, 248.1 $[M+H]^+$, found 248.2 $[M+H]^+$.

2-(4-(3-chloropropyl)piperazin-1-yl)ethan-1-ol (**2ia**)- 1-bromo-3-chloropropane (1.1mL, 1.72g, 11mmol; 1.5eq) of 1-bromo-3-chloropropane and amine component (0.952g, 1eq) were dissolved in acetonitrile (40mL) at room temperature while stirring. triethylamine (3.1mL, 2.2g, 2eq) was then added dropwise, the reaction mixture was stirred at room temperature for 24h and purified as above to yield a yellow oil (yield: 551mg, 36%). LC-MS *m/z*: calculated for $C_9H_{19}ClN_2O+H^+$, 207.1 $[M+H]^+$, found 207.1 $[M+H]^+$.

General synthetic procedure for hydrophilic phenol ether derivatives: 2a (50mg, 0.131mmol, 1eq), the chloropropylamine precursor (2eq), and potassium carbonate (91mg, 0.655mmol, 5eq) were dissolved in dimethyl sulfoxide (6mL). The reaction was heated to reflux overnight (16-20h). The reaction was then cooled to room temperature and 20mL of distilled water was added to the flask. The mixture was added to a separatory funnel and extracted with ethyl acetate (5x30mL). The organic layers were combined and washed with brine (30mL) before concentrating the organic layers under reduced pressure. The crude product was purified with normal phase silica gel chromatography (DCM/MeOH 100/0 to 80/20) to yield the pure solid.

9-(benzo[d][1,3]dioxol-5-yl)-6,7-dimethoxy-4-(3-morpholinopropoxy)naphtho[2,3-c]furan-1(3H)-one (**2g**)- **2a** (50mg, 0.131mmol, 1eq), **2ga** (22mg, 2eq), and potassium carbonate (80mg, 0.579mmol, 5eq) were dissolved in dimethyl sulfoxide (6mL). The reaction was heated to reflux overnight and purified as above to give a yellow solid (yield: 45mg, 67%, Purity: 95.2%). ^{1}H NMR (500 MHz, DMSO-d_6) δ 7.49 (s, 1H), 7.00 (d, *J* = 7.9 Hz, 1H), 6.93 (s, 1H), 6.85 (d, *J* = 1.6 Hz, 1H), 6.73 (dd, *J* = 7.9, 1.7 Hz, 1H), 6.09 (s, 2H), 5.58 (s, 2H), 4.27 (t, *J* = 6.1 Hz, 2H), 3.92 (s, 3H), 3.63 (s, 3H), 3.55 (t, *J* = 4.5 Hz, 4H), 2.53 (t, *J* = 7.3 Hz, 2H), 2.36 (s, 4H), 1.97 (p, *J* = 6.6 Hz, 2H). ^{13}C NMR (201 MHz, DMSO-d_6) δ 169.5, 151.7, 150.4, 147.4, 147.3, 146.9, 133.3, 130.0, 128.8, 126.0, 125.8, 124.1, 119.4, 111.3, 108.4, 106.0, 101.6, 101.0, 70.4, 67.1, 66.7, 56.0, 55.7, 55.4, 53.9, 27.3. ESI-MS (ESI+) *m/z*: calculated for $C_{28}H_{29}NO_8+H^+$, 508.1966 $[M+H]^+$, found 508.1967 $[M+H]^+$.

Ethyl 2-(4-(3-((9-(benzo[d][1,3]dioxol-5-yl)-6,7-dimethoxy-1-oxo-1,3-dihydronaphtho[2,3-c]furan-4-yl)oxy)propyl)piperazin-1-yl)acetate (**2h**)- **2a** (51mg, 0.134mmol, 1eq), **2ha** (33mg, 2eq), and potassium carbonate (90mg, 0.655mmol, 5eq) were dissolved in dimethyl sulfoxide (6mL). The reaction was heated to reflux overnight and purified as above to give an off-white, amorphous solid (yield: 36mg, 46%, Purity: 97.1%). ^{1}H NMR (500 MHz, DMSO-d_6) δ 7.47 (s, 1H), 6.99 (d, *J* = 7.9 Hz, 1H), 6.92 (s, 1H), 6.84 (d, *J* = 1.6 Hz, 1H), 6.72 (dd, *J* = 8.0, 1.7 Hz, 1H), 6.09 (s, 2H), 5.56 (s, 2H), 4.24 (t, *J* = 6.1 Hz, 2H), 4.04 (q, *J* = 7.1 Hz, 2H), 3.91 (s, 3H), 3.62 (s, 3H), 3.15 (s, 2H), 2.59 – 2.53 (m, 2H), 2.50 (s, 8H), 1.96 (p, J = 6.6 Hz, 2H), 1.14 (t, *J* = 7.1 Hz, 3H). ^{13}C NMR (201 MHz, DMSO-d_6) δ 170.2, 169.4, 151.5, 147.2, 147.1, 146.7, 133.2, 129.8, 128.7, 125.9, 125.7, 123.9, 119.3, 111.2, 108.2, 105.8, 101.4, 100.8, 70.3, 66.9, 60.1, 58.8, 55.9, 55.5, 53.1, 52.3, 40.7, 27.3, 14.5. ESI-MS (ESI+) *m/z*: calculated for $C_{32}H_{36}N_2O_9+H^+$, 593.2493 $[M+H]^+$, found 593.2491 $[M+H]^+$.

9-(benzo[d][1,3]dioxol-5-yl)-4-(3-(4-(2-hydroxyethyl)piperazin-1-yl)propoxy)-6,7-dimethoxynaphtho[2,3-c]furan-1(3H)-one (**2i**)- **2a** (51mg, 0.131mmol, 1eq), **2ia** (27mg, 2eq), and potassium carbonate (90mg, 0.655mmol, 5eq) were dissolved in dimethyl sulfoxide (6mL). The reaction was heated to reflux overnight and purified as above to give a yellow, amorphous solid (Yield: 32mg, 44%, Purity: 95.1%). ^{1}H NMR (500 MHz, DMSO-d_6) δ 7.48 (s, 1H), 7.00 (d, *J* = 7.9 Hz, 1H), 6.93 (s, 1H), 6.73 (dd, *J* = 7.9, 1.7 Hz, 1H), 6.09 (s, 2H), 5.57 (s, 2H), 4.42 (s, 1H), 4.26 (t, *J* = 6.0 Hz, 2H), 3.92 (s, 3H), 3.62 (s, 3H), 3.46 (t, *J* = 6.3 Hz, 2H), 2.57 – 2.48 (m, 4H), 2.38 (s, 8H), 1.96 (p, *J* = 6.6 Hz, 2H). ^{13}C NMR (126 MHz, DMSO-d_6) δ 169.4, 151.5, 150.2, 147.2, 147.1, 146.7, 133.2, 129.8, 128.7, 125.9, 125.7, 123.9, 119.3, 111.2, 108.3, 105.8, 101.4, 100.8, 70.3, 66.9, 60.5, 58.6, 55.9, 55.5, 54.8, 53.4, 53.0, 27.4. ESI-MS (ESI+) *m/z*: calculated for $C_{30}H_{34}N_2O_7+H^+$, 551.2388 $[M+H]^+$, found 551.2383 $[M+H]^+$.

2-amino-9-(benzo[d][1,3]dioxol-5-yl)-4-hydroxy-6,7-dimethoxy-2,3-dihydro-1H-benzo[f]isoindol-1-one (**3a**)- **2a** (200mg, 0.526mmol, 1eq) and hydrazine hydrate (0.5mL) were dissolved in 50mL of methanol. The reaction was heated to reflux overnight (16-20h). The solution was cooled to -20°C and the precipitate that formed was collected. The crude product was recrystallized with ethanol to yield 136mg (66%, Purity: 96.1%) of **3a** as a yellow solid. ^{1}H NMR (500 MHz, DMSO-d_6) δ 9.98 (s, 1H), 7.56 (s, 1H), 6.93 (d, *J* = 7.8 Hz, 1H), 6.88 (s, 1H), 6.75 (d, *J* = 1.7 Hz, 1H), 6.66 (dd, *J* = 7.9, 1.6 Hz, 1H), 6.06 (d, *J* = 1.9 Hz, 2H), 4.78 (s, 2H), 4.42 (s, 2H), 3.88 (s, 3H), 3.59 (s, 3H). ESI-MS (ESI+) *m/z*: calculated for $C_{21}H_{18}N_2O_6+H^+$, 395.1237 $[M+H]^+$, found 395.1240 $[M+H]^+$.

Hydrazone synthesis: General Procedure. 3a (50mg, 0.126mmol, 1eq) and the select aromatic aldehyde (1.2eq) were dissolved in methanol (10mL). The reaction was heated to reflux overnight (16-20h). The reaction was then cooled to room temperature and concentrated under reduced pressure. The residual solution was then cooled to -20°C to precipitate the crude product from solution. The crude precipitate was collected and recrystallized with ethanol to yield the final product.

(E)-9-(benzo[d][1,3]dioxol-5-yl)-2-(benzylideneamino)-4-hydroxy-6,7-dimethoxy-2,3-dihydro-1H-benzo[f]isoindol-1-one (**3b**)- **3a** (50mg, 0.126mmol, 1eq) and benzaldehyde (15µl 16mg, 1.2eq) were dissolved in methanol (10mL). The reaction was heated to reflux overnight, and the final product was purified as above to give a yellow solid (yield**:** 52mg, 85%, Purity: 96.2%). ^{1}H NMR (500 MHz, DMSO-d_6) δ 10.22 (s, 1H), 8.65 – 8.61 (m, 2H), 8.10 (s, 1H), 7.64 (d, *J* = 5.2 Hz, 4H), 6.98 (d, *J* = 8.0 Hz, 1H), 6.92 (s, 1H), 6.83 (s, 1H), 6.72 (d, *J* = 8.0 Hz, 1H), 6.09 (s, 2H), 4.84 (s, 2H), 3.90 (s, 3H), 3.61 (s, 3H). ESI-MS (ESI+) *m/z*: calculated for $C_{28}H_{22}N_2O_6$ $+H^+$, 483.1551 $[M+H]^+$, found 483.1547 $[M+H]^+$.

(E)-9-(benzo[d][1,3]dioxol-5-yl)-4-hydroxy-6,7-dimethoxy-2-((pyridin-3-ylmethylene)amino)-2,3-dihydro-1H-benzo[f]isoindol-1-one (**3c**)- **3a** (50mg, 0.126mmol, 1eq) and nicotinaldehyde (14µl, 16mg, 1.2eq) were dissolved in methanol (10mL). The reaction was heated to reflux overnight, and the final product was purified as above to give a yellow solid (yield**:** 45mg, 74%, Purity: 95.5%). ^{1}H NMR (300 MHz, DMSO-d_6) δ 10.24 (s, 1H), 8.90 (s, 1H), 8.60 (s, 1H), 8.23 (s, 1H), 8.13 (d, *J* = 8.1 Hz, 1H), 7.67 (s, 1H), 7.56 – 7.45 (m, 1H), 7.06 – 6.91 (m, 2H), 6.86 (d, *J* = 1.6 Hz, 1H), 6.75 (d, *J* = 8.1 Hz, 1H), 6.11 (s, 2H), 4.88 (s, 2H), 3.93 (s, 3H), 3.64 (s, 3H), 1.90 (s, 1H). ^{13}C NMR (201 MHz, DMSO-d_6) δ 164.0, 150.9, 150.5, 149.9, 149.2, 147.2, 146.8, 146.0, 140.7, 133.7, 131.2, 130.1, 129.7, 129.1, 124.5, 124.2, 123.2, 115.8, 111.7, 108.1, 106.0, 101.5, 101.4, 56.0, 55.5, 45.5, 21.5. ESI-MS (ESI+) *m/z*: calculated for $C_{27}H_{21}N_3O_6$ $+H^+$, 483.1503 $[M+H]^+$, found 483.1500 $[M+H]^+$.

(E)-9-(benzo[d][1,3]dioxol-5-yl)-2-((4-chlorobenzylidene)amino)-4-hydroxy-6,7-dimethoxy-2,3-dihydro-1H-benzo[f]isoindol-1-one (**3d**)- **3a** (49mg, 0.124mmol, 1eq) and 4-chlorobenzaldehyde (21mg, 1.2eq) were dissolved in methanol (10mL). The reaction was heated to reflux overnight, and the final product was purified as above to give a yellow solid (yield**:** 51mg, 77%, Purity: 99.2%). ^{1}H NMR (500 MHz, DMSO-d_6) δ 10.19 (s, 1H), 8.16 (s, 1H), 7.75 (d, *J* = 8.6 Hz, 2H), 7.64 (s, 1H), 7.55 – 7.48 (m, 2H), 6.98 (d, *J* = 7.9 Hz, 1H), 6.91 (s, 1H), 6.82 (d, *J* = 1.7 Hz, 1H), 6.72 (dd, *J* = 7.9, 1.7 Hz, 1H), 6.08 (s, 2H), 4.84 (s, 2H), 3.91 (s, 3H), 3.61 (s, 3H). ESI-MS (ESI+) *m/z*: calculated for $C_{28}H_{21}ClN_2O_6$ $+H^+$, 517.1161 $[M+H]^+$, found 517.1156 $[M+H]^+$.

(E)-9-(benzo[d][1,3]dioxol-5-yl)-2-((4-bromobenzylidene)amino)-4-hydroxy-6,7-dimethoxy-2,3-dihydro-1H-benzo[f]isoindol-1-one (**3e**)- **3a** (50mg, 0.126mmol, 1eq) and 4-bromobenzaldehyde (28mg, 1.2eq) were dissolved in methanol (10mL). The reaction was heated to reflux overnight, and the final product was purified as above to give a yellow solid (yield**:** 55mg, 76%, Purity: 97.9%). ^{1}H NMR (300 MHz, DMSO-d_6) δ 10.23 (s, 1H), 8.16 (s, 1H), 7.68 (dd, *J* = 5.8, 2.9 Hz, 5H), 7.05 – 6.89 (m, 2H), 6.88 – 6.69 (m, 2H), 6.11 (s, 2H), 4.86 (s, 2H), 3.93 (s, 3H), 3.63 (s, 3H). LC-MS m/z: calculated for $C_{28}H_{21}BrN_2O_6+H^+$, 561.1 $[M+H]^+$, found 561.4 $[M+H]^+$.

(E)-9-(benzo[d][1,3]dioxol-5-yl)-4-hydroxy-6,7-dimethoxy-2-((4-methylbenzylidene)amino)-2,3-dihydro-1H-benzo[f]isoindol-1-one (**3f**)- **3a** (49mg, 0.124mmol, 1eq) and 4-methylbenzaldehyde (18µl, 18mg, 1.2eq) were dissolved in methanol (10mL). The reaction was heated to reflux overnight, and the final product was purified as above to give a yellow solid (yield**:** 39mg, 62%, Purity: 97.3%). ^{1}H NMR (500 MHz, DMSO-d_6) δ 10.17 (s, 1H), 8.10 (s, 1H), 7.61 (d, *J* = 6.9 Hz, 3H), 7.24 (d, *J* = 7.7 Hz, 2H), 6.98 (d, *J* = 7.9 Hz, 1H), 6.91 (s, 1H), 6.82 (s, 1H), 6.71 (d, *J* = 7.9 Hz, 1H), 6.08 (s, 2H), 4.80 (s, 2H), 3.90 (s, 3H), 3.60 (s, 3H), 2.30 (s, 3H). LC-MS *m/z*: calculated for $C_{29}H_{24}N_2O_6+H^+$, 497.2 $[M+H]^+$, found 497.3 $[M+H]^+$.

(E)-4-(((9-(benzo[d][1,3]dioxol-5-yl)-4-hydroxy-6,7-dimethoxy-1-oxo-1,3-dihydro-2H-benzo[f]isoindol-2-yl)imino)methyl)benzonitrile (**3g**)-

3a (51mg, 0.129mmol, 1eq) and 4-formylbenzonitrile (17mg, 1.2eq) were dissolved in methanol (10mL). The reaction was heated to reflux overnight, and the final product was purified as above to give a yellow solid (yield**:** 30mg, 47%, Purity: 98.1%). ^{1}H NMR (300 MHz, DMSO-d_6) δ 10.22 (s, 1H), 8.17 (s, 1H), 7.65 (s, 1H), 7.01 (d, *J* = 7.9 Hz, 1H), 6.93 (s, 1H), 6.90 – 6.84 (m, 1H), 6.80 – 6.70 (m, 1H), 6.12 (s, 2H), 4.83 (s, 2H), 3.92 (s, 3H), 3.64 (s, 3H). ^{13}C NMR (201 MHz, DMSO-d_6) δ 164.1, 150.5, 149.9, 147.2, 146.8, 146.0, 141.3, 139.7, 133.2, 130.0, 129.7, 129.2, 127.9, 124.3, 124.2, 123.3, 119.2, 115.8, 111.9, 111.7, 108.1, 106.0, 101.4, 101.4, 56.0, 55.5, 45.5. ESI-MS (ESI+) *m/z*: calculated for $C_{29}H_{23}N_3O_6$+H$^+$, 508.1500 [M+H]$^+$, found 508.1503 [M+H]$^+$.

(E)-9-(benzo[d][1,3]dioxol-5-yl)-4-hydroxy-6,7-dimethoxy-2-(((perfluorophenyl)methylene)amino)-2,3-dihydro-1H-benzo[f]isoindol-1-one (**3h**)- **3a** (51mg, 0.129mmol, 1eq) and 2,3,4,5,6-pentafluorobenzaldehyde (19µl, 30mg, 1.2eq) were dissolved in methanol (10mL). The reaction was heated to reflux overnight, and the final product was purified as above to give a white solid (yield**:** 64mg, 88%, Purity: 98.9%). ^{1}H NMR (300 MHz, DMSO-d_6) δ 10.41 (s, 1H), 7.65 (s, 1H), 7.12 – 6.57 (m, 5H), 6.12 (s, 2H), 3.94 (s, 3H), 3.65 (s, 3H), 3.17 (s, 2H). ESI-MS (ESI+) *m/z*: calculated for $C_{28}H_{17}F_5N_2O_6$+H$^+$, 573.1079 [M+H]$^+$, found 573.1077 [M+H]$^+$.

(E)-9-(benzo[d][1,3]dioxol-5-yl)-2-((4-(diethylamino)benzylidene)amino)-4-hydroxy-6,7-dimethoxy-2,3-dihydro-1H-benzo[f]isoindol-1-one (**3i**)- **3a** (50mg, 0.126mmol, 1eq) and 4-(diethylamino)benzaldehyde (27mg, 1.2eq) were dissolved in methanol (10mL). The reaction was heated to reflux overnight, and the final product was purified as above to give a bright yellow solid (yield**:** 45mg, 64%, Purity: 94.9%). ^{1}H NMR (300 MHz, DMSO-d_6) δ 10.15 (s, 1H), 8.07 (s, 1H), 7.64 (s, 1H), 7.54 (d, *J* = 8.7 Hz, 2H), 7.04 – 6.90 (m, 2H), 6.83 (d, *J* = 1.6 Hz, 1H), 6.78 – 6.67 (m, 3H), 6.10 (s, 2H), 4.81 (s, 2H), 3.92 (s, 3H), 3.63 (s, 3H), 3.38 (d, *J* = 7.0 Hz, 4H), 2.53 (s, 11H), 1.10 (t, *J* = 6.9 Hz, 7H). LC-MS m/z: calculated for $C_{32}H_{31}N_3O_6$+H$^+$, calculated 554.2 [M+H]$^+$, found 554.4 [M+H]$^+$.

(E)-9-(benzo[d][1,3]dioxol-5-yl)-2-((benzo[d][1,3]dioxol-5-ylmethylene)amino)-4-hydroxy-6,7-dimethoxy-2,3-dihydro-1H-benzo[f]isoindol-1-one (**3j**)- **3a** (50mg, 0.126mmol, 1eq) and piperonal (23mg, 1.2eq) were dissolved in methanol (10mL). The reaction was heated to reflux overnight, and the final product was purified as above to give a beige solid (yield**:** 55mg, 82%, Purity: 96.1%). ^{1}H NMR (300 MHz, DMSO-d_6) δ 8.11 (s, 1H), 7.65 (d, *J* = 4.2 Hz, 1H), 7.29 (d, *J* = 1.6 Hz, 1H), 7.22 (d, *J* = 8.3 Hz, 1H), 7.00 (dd, *J* = 7.9, 1.7 Hz, 2H), 6.93 (d, *J* = 3.4 Hz, 1H), 6.84 (d, *J* = 1.6 Hz, 1H), 6.73 (dd, *J* = 7.8, 1.7 Hz, 1H), 6.09 (d, *J* = 8.0 Hz, 4H), 4.81 (s, 2H), 3.92 (s, 3H), 3.63 (s, 3H). LC-MS m/z: calculated for $C_{29}H_{22}N_2O_8$+H$^+$, 527.1 [M+H]$^+$, found 527.4 [M+H]$^+$.

(E)-9-(benzo[d][1,3]dioxol-5-yl)-4-hydroxy-6,7-dimethoxy-2-((thiophen-2-ylmethylene)amino)-2,3-dihydro-1H-benzo[f]isoindol-1-one (**3k**)- **3a** (50mg, 0.126mmol, 1eq) and 2-thiophenecarboxaldehyde (14µl, 17mg, 1.2eq) were dissolved in methanol (10mL). The reaction was heated to reflux overnight, and the final product was purified as above to give a beige solid (yield**:** 43mg, 69%, Purity: 96.7%). ^{1}H NMR (500 MHz, DMSO-d_6) δ 8.23 (s, 1H), 7.89 (dd, *J* = 2.9, 1.2 Hz, 1H), 7.69 – 7.56 (m, 2H), 7.43 (dd, *J* = 5.1, 1.2 Hz, 1H), 6.97 (d, *J* = 7.9 Hz, 1H), 6.92 (s, 1H), 6.81 (d, *J* = 1.7 Hz, 1H), 6.71 (dd, *J* = 7.9, 1.7 Hz, 1H), 6.08 (dd, *J* = 3.9, 1.0 Hz, 2H), 4.80 (s, 2H), 3.90 (s, 3H), 3.61 (s, 3H). LC-MS m/z: calculated for $C_{26}H_{20}N_2O_6S$+H$^+$, 489.1 [M+H]$^+$, found 489.1 [M+H]$^+$.

(**E)-9-(benzo[d][1,3]dioxol-5-yl)-4-hydroxy-6,7-dimethoxy-2-((4-(trifluoromethyl)benzylidene)amino)-2,3-dihydro-1H-benzo[f]isoindol-1-one** (**3l**)- **3a** (50mg, 0.126mmol, 1eq) and 4-(trifluoromethyl)benzaldehyde (21µl, 26mg, 1.2eq) were dissolved in methanol (10mL). The reaction was heated to reflux overnight, and the final product was purified as above to give a yellow solid (yield**:** 61mg, 87%, Purity: 99.4%). ^{1}H NMR (500 MHz, DMSO-d_6) δ 10.22 (s, 1H), 8.22 (s, 1H), 7.93 (t, *J* = 9.0 Hz, 2H), 7.82 (d, *J* = 8.1 Hz, 2H), 7.65 (s, 1H), 6.99 (d, *J* = 7.7 Hz, 1H), 6.92 (s, 1H), 6.82 (d, *J* = 11.5 Hz, 1H), 6.72 (d, *J* = 8.0 Hz, 1H), 6.09 (s, 2H), 4.87 (s, 1H), 3.91 (s, 3H), 3.61 (s, 3H). LC-MS: m/z: calculated for $C_{29}H_{21}F_3N_2O_6$+H$^+$, 551.2 [M+H]$^+$, found 551.2 [M+H]$^+$.

Ring-opened amide synthesis: General Procedure. 2a (50mg, .131mmol, 1eq) and the amine component (2eq) were dissolved in a 0.5M NaOH in MeOH solution (5mL). The reaction was heated to reflux overnight (16-20h). The reaction was then cooled to room temperature and the solvent was removed under reduced pressure. The reaction was then suspended in 10mL of distilled water and the pH was adjusted to 7. The solution was then added to a separatory funnel and extracted with ethyl acetate (3x30mL). The organic layers were combined and washed with distilled water (30mL) and brine (30mL) before being concentrated under reduced pressure. The crude product was purified using normal phase silica gel chromatography (DCM/MeOH 100/0 to 80/20) to yield the final product.

(1-(benzo[d][1,3]dioxol-5-yl)-4-hydroxy-3-(hydroxymethyl)-6,7-dimethoxynaphthalen-2-yl)(piperidin-1-yl)methanone (**4a**)- **2a** (50mg, .131mmol, 1eq) and the piperidine (26µl, 22mg, 2eq) were dissolved in a 0.5M NaOH in MeOH solution (5mL). The reaction was heated to reflux overnight and purified as shown above to yield a yellow solid (yield**:** 35mg, 57%, Purity: 95.1%). ^{1}H NMR (500 MHz, DMSO-d_6) δ 7.41 – 7.37 (m, 1H), 7.13 (d, *J* = 1.7 Hz, 1H), 7.00 (d, *J* = 8.2 Hz, 1H), 6.89 (d, *J* = 8.1 Hz, 1H), 6.80 (s, 1H), 6.13 – 6.05 (m, 2H), 3.82 (s, 3H), 3.75 (s, 3H), 3.59 (d, *J* = 18.3 Hz, 2H), 2.86 – 2.69 (m, 10H). LC-MS m/z: calculated for $C_{23}H_{20}O_7$ +H$^+$, 466.2 [M+H]$^+$, found 466.3 [M+H]$^+$.

(1-(benzo[d][1,3]dioxol-5-yl)-4-hydroxy-3-(hydroxymethyl)-6,7-dimethoxynaphthalen-2-yl)(morpholino)methanone (**4b**)- **2a** (50mg, .131mmol, 1eq) and morpholine (23µl, 23mg, 2eq) were dissolved in a 0.5M NaOH in MeOH solution (5mL). The reaction was heated to reflux overnight and purified as shown above to yield a yellow solid (yield**:** 26mg, 43%, Purity: 95.4%). ^{1}H NMR (500 MHz, DMSO-d_6) δ 7.52 (s, 1H), 6.92 – 6.78 (m, 2H), 5.98 (s, 1H), 5.93 (s, 1H), 5.11 (s, 2H), 3.92 (s, 3H), 3.66 (s, 3H), 3.15 – 3.11 (m, 4H), 2.62 (s, 4H), 2.55 (s, 2H). LC-MS *m/z*: calculated for $C_{25}H_{25}NO_8$+H$^+$, 468.2 [M+H]$^+$, found 468.2 [M+H]$^+$.

(1-(benzo[d][1,3]dioxol-5-yl)-4-hydroxy-3-(hydroxymethyl)-6,7-dimethoxynaphthalen-2-yl)(4-methylpiperazin-1-yl)methanone (**4c**)- **2a** (50mg, .131mmol, 1eq) and N-methylpiperazine (24µl, 21mg, 2eq) were dissolved in a 0.5M NaOH in MeOH solution (5mL). The reaction was heated to reflux overnight and purified as shown above to yield a yellow solid (yield**:** 10mg, 16%, Purity: 94.6%). ^{1}H NMR (500 MHz, DMSO-d_6) δ 8.52 (s, 1H), 7.43 (s, 1H), 7.14 (s, 1H), 6.96 (s, 1H), 6.82 (s, 1H), 6.74 (d, *J* = 8.7 Hz, 1H), 5.94 – 5.84 (m, 2H), 4.98 (s, 2H), 4.06 (s, 1H), 3.74 (s, 3H), 3.20 (s, 3H), 3.03 (s, 8H), 1.20 (s, 3H). LC-MS *m/z*: calculated for $C_{26}H_{28}N_2O_7$+H$^+$, 517.1161 [M+H]$^+$, found 481.2 [M+H]$^+$.

(1-(benzo[d][1,3]dioxol-5-yl)-4-hydroxy-3-(hydroxymethyl)-6,7-dimethoxynaphthalen-2-yl)(piperazin-1-yl)methanone (**4d**)- **2a** (50mg, .131mmol, 1eq) and piperazine (23mg, 2eq) were dissolved in a 0.5M NaOH in MeOH solution (5mL). The reaction was heated to reflux overnight and purified as shown above to yield a yellow solid (yield**:** 12mg, 20%, Purity: 93.2%). ^{1}H NMR (500 MHz, DMSO-d_6) δ 7.65 (s, 1H), 7.09 (s, 1H), 6.97 (d, *J* = 8.7 Hz, 1H), 6.84 (s, 1H), 6.73 (d, *J* = 8.7 Hz, 1H), 6.10 (s, 2H), 5.35 (s, 2H), 3.91 (s, 3H), 3.55 (s, 3H), 2.69 (s, 6H). LC-MS *m/z*: calculated for $C_{25}H_{26}N_2O_7$+H$^+$, 467.2 [M+H]$^+$, found 467.1 [M+H]$^+$.

1-(benzo[d][1,3]dioxol-5-yl)-N-cyclopentyl-4-hydroxy-3-(hydroxymethyl)-6,7-dimethoxy-2-naphthamide (**4e**)- **2a** (50mg, .131mmol, 1eq) and cyclopentylamine (26µl, 23mg, 2eq) were dissolved in a 0.5M NaOH in MeOH solution (5mL). The reaction was heated to reflux overnight and purified as shown above to yield an off-white solid (yield**:** 21mg, 19%, Purity: 96.7%). ^{1}HNMR (500MHz, DMSO-d_6) 7.50(s, 1H), 6.91(s, 1H), 6.75(s, 1H), 6.73(s, 1H), 6.675(d, *J*=5Hz, 1H), 6.03(d, *J* = 20Hz, 2H), 4.03(s, 2H), 3.84(s, 3H), 3.56 (s, 3H), 3.31(b, 1H), 3.21(s, b,1H), 1.84(m, 2H), 1.64(m, 2H), 1.5(m, 4H). LC-MS *m/z*: calculated for $C_{26}H_{27}NO_7$+H$^+$, 466.2 [M+H]$^+$, found 466.1 [M+H]$^+$.

Biological Assays

Cells- 293FT cells (catalog number R700-07; Thermo), HEK-293 cells (ATCC® CRL-1573™), Vero cells and HeLa cells were maintained in Dulbecco modified Eagle medium (Fisher Scientific) supplemented with 10% fetal bovine serum (Atlanta Biologicals) (referred to here as complete medium). Primary human macrophages were differentiated from the buffy coat fraction of human blood (from the South Texas Blood and Tissue Center) according to previously published protocols.[5] Briefly, mononuclear lymphocytes were isolated using LeucoSep tubes (Fisher Scientific), resuspended in Iscove modified Dulbecco medium (IMDM, Fisher Scientific), and plated in 96-well plates (50,000 cells per well). After the cells were allowed to adhere for 1 h, unattached cells were washed off using IMDM. Attached monocytes were allowed to differentiate into macrophages for 7 to 8 days in IMDM containing 2% heat-inactivated human serum (Corning Inc.), 100 U/ml penicillin, 100 µg/ml streptomycin, 1× nonessential amino acids (Fisher Scientific), 50 µM 2-mercaptoethanol (Fisher Scientific), and 800 U/ml human macrophage colony-stimulating factor (BioLegend). Adherent monocytes (PHMs) were washed, and the

medium was replaced on days 2 and 6 while the cells were differentiating. All cells were kept at 37°C in a humidified incubator with 5% CO_2.

Pseudovirus assays- As described previously, Virus-like particles (VLPs) containing ebolavirus glycoprotein (GP) were produced in 293FT cells. Plasmid DNA constructs carrying EBOV or MARV matrix protein VP40, VP40 fused to GFP (VP40-GFP), NP, and GP were used for VLP production.[5] HeLa cells were seeded in a 384-well plate (4000 cells/well) and allowed to adhere overnight in complete medium at 37°C with 5% CO_2. Cells were treated with inhibitors at varying concentrations (<1% DMSO) for 1 h before the cells were infected with EBOV or MARV pseudovirus. After 24 h, cells were fixed with formalin and washed three times with phosphate-buffered saline. Nuclei were then stained with Hoechst stain at a concentration of 1:10,000. Cells were imaged using a Nikon Ti eclipse robotic microscope and analyzed with CellProfiler software. The number of infected cells (GFP-expressing cells) was divided by the total number of cells (Hoechst-stained nuclei) to determine the rate of infection. The infection rate in vehicle-treated cells was used to determine the ratio of infection in the drug-treated cells. IC_{50} data are reported as the concentration at which 50% of the viral infection was inhibited relative to the vehicle-treated cells with the standard deviation for 6 individual experiments.

Filovirus-GFP infection- Live EBOV were produced as previously described.[5] In brief, Zaire Ebola virus Mayinga strain with an insertion of green fluorescent protein (GFP) between the nucleoprotein (NP) and VP35, a kind gift of Heinz Feldmann (NIH, Rocky Mountain Laboratory, Hamilton, MT). All work was done in a biosafety level 4 (BSL4; protection level 4) lab at the Texas Biomedical Research Institute.
PHMs were treated with inhibitors at varying concentrations (<1% DMSO) for 1 h before the cells were infected with EBOV-GFP. After 24 h, cells were fixed with formalin and washed three times with phosphate-buffered saline. Nuclei were then stained with Hoechst stain at a concentration of 1:10,000. Cells were imaged using a Nikon Ti eclipse robotic microscope and analyzed with CellProfiler software. The number of infected cells (GFP-expressing cells) was divided by the total number of cells (Hoechst-stained nuclei) to determine the rate of infection. The infection rate in vehicle-treated cells was used to determine the ratio of infection in the drug-treated cells. IC_{50} data are reported as the concentration at which 50% of the viral infection was inhibited relative to the controls with the standard deviation for 6 individual experiments.

Inhibition of cellular vesicle acidification- HEK-293 cells were seeded into clear 96-well plates (Falcon) at 10,000 cells/well and allowed to grow for 18-20 h at 37°C and 5% CO_2 in complete medium. Cells were treated with inhibitors at varying concentrations (<2% DMSO) for 4 h before the addition of 1 µg/ml acridine orange in DMEM for 10min before media is removed and cells washed twice with 1x PBS. Fluorescent readings were taken with a Biotek Synergy 4 microplate reader using the following filter pairings: 485/20 nm-530/30 nm and 485/20 nm-665/7 nm. Data are shown the 665 nm/530 nm emission ratio for 12 individual experiments. IC_{50} data are reported as the concentration at which 50% of the 665 nm/ 530 nm ratio was inhibited relative to the vehicle-treated control with the standard deviation. All compounds were also assayed without the acridine orange dye to determine if background fluorescence was interfering with the assay. This background fluorescence was determined by washing cells with 1x PBS twice and reading in both fluorescence wavelengths and subtracted from the total fluorescence in both channels before determining the fluorescent ratio after dye treatment.

Aggregation screening for cellular endosomal acidification- All hits from the cellular endosomal acidification assay were further screened at 10µM under two different conditions to eliminate any compounds that inhibit the assay by aggregation. The first condition was the addition of 0.1% Triton X-100 as inhibitors were added to HEK-293 cells. The assay was run for 4h before 1 µg/ml acridine orange in DMEM was added with 0.1% Triton X-100 to additionally inhibit any aggregation between dye and inhibitors. The second condition was to add inhibitors to assay media and centrifuge them for 10min at 14,000x*g* to remove aggregates before adding inhibitors to HEK-293 cells. The assay was conducted as above.

Time-dependent inhibition of cellular vesicle acidification- HEK-293 cells were seeded into clear 96-well plates (Falcon) at 10,000 cells/well and allowed to grow for 18-20 h at 37°C and 5% CO_2 in complete medium. Cells were then treated with a dilution series of diphyllin and incubated at 37°C and 5%CO_2 until 1 µg/ml acridine orange was added at 2, 4, and 8h. After 10min incubation the dye, cells were washed with 1x PBS twice and 100µl of PBS was added. Fluorescent readings were taken with a Biotek Synergy 4 microplate reader using the following filter pairings: 485/20 nm-530/30 nm and 485/20 nm-665/7 nm. Data are shown as mean± standard error of the mean of the 665 nm/530 nm emission ratio for 4 individual experiments.

Measurement of intracellular endosomal pH- HEK-293 cells were seeded into clear 96-well plates (Falcon) at 10,000 cells/well and allowed to grow for 18-20 h at 37°C and 5% CO_2 in complete medium. Cells were then incubated with 0.5 mg/ml FITC-dextran for 3 h. The dextran was then removed and the cells washed once with 1x PBS before the addition of inhibitors (<2% DMSO) in DMEM for 4 h. Cell were then washed 1x with PBS and read with a Biotek Synergy 4 microplate reader with the 485/20 nm and 380/20nm excitation filters and the 530/30 nm emission filter. The 380 nm induced emission was subtracted from the 485 nm induced emission to normalize the results for dye concentration. Data are shown as mean± standard error of the mean of the normalized 530nm emission for 12 individual experiments. FITC-dextran fluorescence was standardized in vehicle-treated cells using HEPES-phosphate buffers with 10 µg/ml of nigericin at pH values from 4-8 for a standard curve. The ionophore nigericin was added to equilibrate the cell's internal pH with the external buffer pH.

Measurement of cytosolic pH- HEK-293 cells were seeded into clear 96-well plates (Falcon) at 10,000 cells/well and allowed to grow for 18-20 h at 37°C and 5% CO_2 in complete medium. Cells were then treated with inhibitors at varying concentrations (<2% DMSO) for 3.5 h before the addition of 10 µg/ml of BCECF-AM. After 30 min, cells were washed twice with 1xPBS before reading the plate with a Biotek Synergy 4 microplate reader with the 485/20 nm and 380/20nm excitation filters and the 530/30 nm emission filter. The 380 nm induced emission was subtracted from the 485 nm induced emission to normalize the results for dye concentration. Data are shown as mean± standard error of the mean of the normalized 530 nm emission for 12 individual experiments. BCECF-AM fluorescence was standardized in vehicle-treated cells using HEPES-phosphate buffers with 10 µg/ml of nigericin at pH values from 4-8 for a standard curve. The ionophore nigericin was added to equilibrate the cell's internal pH with the external buffer pH.

Determination of cytotoxicity- HEK-293 cells were seeded into clear 96-well plates (Falcon) at 10,000 cells/well and allowed to grow for 18-20 h at 37°C and 5% CO_2 in complete medium. Cells were then treated with inhibitors at varying concentrations (<2%DMSO) for 72 h. 0.5 mg/ml MTT was added to cells for 4 h before quenching the reaction with acidic isopropanol (10% Triton, 0.1 M HCl). After incubation for 24 h at room temperature, the absorbance at 570 nm and 650 nm was measured using a Biotek Synergy 4 microplate reader. The absorbance at 650 nm subtracted from the 570 nm to normalize data to any residual media fluorescence. Data are shown as mean± standard error of the mean of the normalized 570nm absorbance. CC_{50} data are reported as the concentration at which cell viability was 50% relative to the controls with the standard deviation for 12 individual experiments.
HeLa cytotoxicity was determined as shown previously.[5] In brief, HeLa cells plated in 96-well plates (20,000 cells/well) were treated with the compounds at different concentrations in a 100 µl final volume. After 24 h of incubation with the compounds, cytotoxicity was measured using a CytoTox-Fluor cytotoxicity assay (Promega) per the manufacturer's protocol.
PHM cytotoxicity was determined as shown previously.[5] In brief, PHMs were treated with the top three diphyllin derivatives at varying concentrations (<1% DMSO). After 24 h of incubation with the compounds, cytotoxicity was measured using a CytoTox-Fluor cytotoxicity assay (Promega) per the manufacturer's protocol for 3 individual experiments.

HEK-293 vesicle isolation- The following isolation and assays were performed similar to that previously described.[44,47] In brief, cells were grown to confluency with complete medium in a 175 cm^2 flask (Corning) before growth media was removed and replaced with serum-free DMEM for 2 h. To neutralize endosomes prior to lysis, FCCP was added to the cellular media to reach a final concentration of 1 µM. Cells were incubated with FCCP for 15 min before cells were scrapped form the plate and pelleted at 1000x*g* for 5 min. The media was discarded and cells were re-suspended in HEK assay buffer (20 mM HEPES, 5 mM Glucose, 50 mM Sucrose, 50 mM KCl, 90 mM potassium gluconate, 1 mM EGTA, Pierce™ protease inhibitor Mini tablet, pH=7.4) were then lysed by passage through a 22g needle 10-15 times. Lysates were then centrifuged at 10,000x*g* for 30 s with a Beckman Coulter Microfuge 22R centrifuge. The supernatant was removed and centrifuged at 14,500x*g* for 20 min. The remaining supernatant was discarded and the pellet was resuspended in HEK assay buffer.

Inhibition of acridine orange quenching assay-The vesicle mixture was resuspended in HEK assay buffer+1%BSA+6 µM acridine orange and split

into fractions with the protein concentration being 100 µg/mL and transferred to a clear 96-well plate. The isolated vesicles were pretreated with inhibitors for 60 min at 37°C. Fluorescent readings were taken with a Biotek Synergy 4 microplate reader with the 485/20 nm excitation filter and the 530/30 nm emission filter. Plates were read at 1 min intervals for 2 min to measure baseline fluorescence before 5 mM ATP and 5 mM $MgCl_2$ were added to initiate V-ATPase activity. Readings were taken at 1 min intervals for 60 min before the addition of 1 µg/ml nigericin (Tocris) and further reading for 15 min at 1 min intervals. The change in fluorescence between the 60-minute timepoint after ATP addition and the reading 2 min after nigericin was added were used to quantify the activity of V-ATPase in each sample. Data are shown as mean± standard deviation of nine individual experiments for each compound and concentration.

Inhibition of ATPase activity- The vesicle mixture was resuspended in HEK assay buffer and split into fractions with the protein concentration being 300 µg/mL in 97.5 µl of buffer and transferred to a clear 96-well plate. Vesicles were pretreated with inhibitors (DMSO<1%) for 1hr at 37°C in the presence of 2 mM NaN_3 and 100 µM sodium orthovanadate. The reaction was initiated by the addition of 2.5 µl of 100 mM ATP+100 mM $MgCl_2$ (5 mM ATP+5 mM $MgCl_2$ in solution). 10 µl aliquots of the reaction were added to 90 µl of P_i detection mixture (0.0135% malachite green, 0.954% ammonium molybdate, 0.387% polyvinyl alcohol, 1 M HCl in water) after 60 minutes. After 2 minutes, 10 µl of 34% sodium citrate was added to quench the reaction. After a 30min incubation at room temperature, the absorbance at 620 nm was read using a Biotek Synergy 4 microplate reader. Data are shown as mean± standard error of the mean of the 620nm absorbance for nine individual experiments per compound.

Stability in cell media assessment- Compounds were suspended in DMEM+10%FBS at 100mM concentration and aliquots were removed at 0, 4, 24, 48h while incubating 37°C with 5% CO_2. Sample media was diluted 1/10 in acetonitrile+0.1% trifluoroacetic acid and cooled to 4°C for 30 min. Samples were then centrifuged at 14,000x*g* and the supernatant was removed and analyzed by HPLC using a Phenomenex Kromasil C18 HPLC column. The percentage of the original sample peak was used to determine the amount of compound remaining at each time point in comparison with phenol standard. Data shown are the mean± standard error of the mean for five individual experiments.

Stability in HEK-293 cells- HEK-293 cells were seeded into Corning 6-well plates at a concentration of $5x10^5$ cells/well in DMEM+10% FBS and incubated overnight at 37°C with 5% CO_2. The media was then removed and replaced with DMEM+10% FBS containing 100mM of select inhibitors and allowed to incubate for 24h at 37°C with 5% CO_2. Media was then collected and cells were washed three times with cold PBS before being allowed to dry for 15min. A 1:1:0.0005 mixture of acetonitrile: methanol: trifluoroacetic acid was then added to each well and incubated at 4°C for 16 h. The supernatant was then removed and centrifuged at 14,000x*g* for 10min to remove cellular debris. The new supernatant was then concentrated to 500uL and analyzed by HPLC using Phenomenex Kromasil C18 HPLC column. Data shown are the average of 3 independent experiments.

Acknowledgements

The authors wish to thank Dr. Dino Petrov and Ryan DiFalco for their efforts to improve protocols for scale up of diphyllin synthesis.

Keywords: Diphyllin, Ebolavirus inhibitors, Vacuolar-ATPase, Phenotypic Screening

References:

(1) Ansari, A. A. Clinical Features and Pathobiology of Ebolavirus Infection. *J. Autoimmun.* **2014**, *55*, 1–9.

(2) Messaoudi, I.; Amarasinghe, G. K.; Basler, C. F. Filovirus Pathogenesis and Immune Evasion: Insights from Ebola Virus and Marburg Virus. *Nat. Rev. Microbiol.* **2015**, *13* (11), 663–676.

(3) White, J. M.; Schornberg, K. L. A New Player in the Puzzle of Filovirus Entry. *Nat. Rev. Microbiol.* **2012**, *10* (5), 317–322.

(4) 2014-2016 Ebola Outbreak in West Africa | Ebola Hemorrhagic Fever | CDC http://www.cdc.gov/vhf/ebola/outbreaks/2014-west-africa/index.html (accessed Nov 26, 2016).

(5) Anantpadma, M.; Kouznetsova, J.; Wang, H.; Huang, R.; Kolokoltsov, A.; Guha, R.; Lindstrom, A. R.; Shtanko, O.; Simeonov, A.; Maloney, D. J.; et al. Large Scale Screening and Identification of Novel Ebolavirus and Marburgvirus Entry Inhibitors. *Antimicrob. Agents Chemother.* **2016**, AAC.00543-16.

(6) Basu, A.; Mills, D. M.; Mitchell, D.; Ndungo, E.; Williams, J. D.; Herbert, A. S.; Dye, J. M.; Moir, D. T.; Chandran, K.; Patterson, J. L.; et al. Novel Small Molecule Entry Inhibitors of Ebola Virus. *J. Infect. Dis.* **2015**, *212* (suppl 2), S425–S434.

(7) van der Linden, W. A.; Schulze, C. J.; Herbert, A. S.; Krause, T. B.; Wirchnianski, A. A.; Dye, J. M.; Chandran, K.; Bogyo, M. Cysteine Cathepsin Inhibitors as Anti-Ebola Agents. *ACS Infect. Dis.* **2016**, *2* (3), 173–179.

(8) Luthra, P.; Liang, J.; Pietzsch, C. A.; Khadka, S.; Edwards, M. R.; Wei, S.; De, S.; Posner, B.; Bukreyev, A.; Ready, J. M.; et al. A High Throughput Screen Identifies Benzoquinoline Compounds as Inhibitors of Ebola Virus Replication. *Antiviral Res.* **2018**, *150*, 193–201.

(9) Yates, M. K.; Raje, M. R.; Chatterjee, P.; Spiropoulou, C. F.; Bavari, S.; Flint, M.; Soloveva, V.; Seley-Radtke, K. L. Flex-Nucleoside Analogues – Novel Therapeutics against Filoviruses. *Bioorg. Med. Chem. Lett.* **2017**, *27* (12), 2800–2802.

(10) Selaković, Ž.; Soloveva, V.; Gharaibeh, D. N.; Wells, J.; Šegan, S.; Panchal, R. G.; Šolaja, B. A. Anti-Ebola Activity of Diazachrysene Small Molecules. *ACS Infect. Dis.* **2015**, *1* (6), 264–271.

(11) Bixler, S. L.; Bocan, T. M.; Wells, J.; Wetzel, K. S.; Van Tongeren, S. A.; Dong, L.; Garza, N. L.; Donnelly, G.; Cazares, L. H.; Nuss, J.; et al. Efficacy of Favipiravir (T-705) in Nonhuman Primates Infected with Ebola Virus or Marburg Virus. *Antiviral Res.* **2018**, *151*, 97–104.

(12) Salata, C.; Baritussio, A.; Munegato, D.; Calistri, A.; Ha, H. R.; Bigler, L.; Fabris, F.; Parolin, C.; Palù, G.; Mirazimi, A. Amiodarone and Metabolite MDEA Inhibit Ebola Virus Infection by Interfering with the Viral Entry Process. *Pathog. Dis.* **2015**, *73* (5).

(13) Madrid, P. B.; Panchal, R. G.; Warren, T. K.; Shurtleff, A. C.; Endsley, A. N.; Green, C. E.; Kolokoltsov, A.; Davey, R.; Manger, I. D.; Gilfillan, L.; et al. Evaluation of Ebola Virus Inhibitors for Drug Repurposing. *ACS Infect. Dis.* **2015**, *1* (7), 317–326.

(14) Johansen, L. M.; DeWald, L. E.; Shoemaker, C. J.; Hoffstrom, B. G.; Lear-Rooney, C. M.; Stossel, A.; Nelson, E.; Delos, S. E.; Simmons, J. A.; Grenier, J. M.; et al. A Screen of Approved Drugs and Molecular Probes Identifies Therapeutics with Anti–Ebola Virus Activity. *Sci. Transl. Med.* **2015**, *7* (290), 290ra89-290ra89.

(15) Kouznetsova, J.; Sun, W.; Martínez-Romero, C.; Tawa, G.; Shinn, P.; Chen, C. Z.; Schimmer, A.; Sanderson, P.; McKew, J. C.; Zheng, W.; et al. Identification of 53 Compounds That Block Ebola Virus-like Particle Entry via a Repurposing Screen of Approved Drugs. *Emerg. Microbes Infect.* **2014**, *3* (12), e84.

(16) Johansen, L. M.; Brannan, J. M.; Delos, S. E.; Shoemaker, C. J.; Stossel, A.; Lear, C.; Hoffstrom, B. G.; DeWald, L. E.; Schornberg, K. L.; Scully, C.; et al. FDA-Approved Selective Estrogen Receptor Modulators Inhibit Ebola Virus Infection. *Sci. Transl. Med.* **2013**, *5* (190), 190ra79-190ra79.

(17) Reynolds, P.; Marzi, A. Ebola and Marburg Virus Vaccines. *Virus Genes* **2017**, 1–15.

(18) Mire, C. E.; Matassov, D.; Geisbert, J. B.; Latham, T. E.; Agans, K. N.; Xu, R.; Ota-Setlik, A.; Egan, M. A.; Fenton, K. A.; Clarke, D. K.; et al. Single-Dose Attenuated Vesiculovax Vaccines Protect Primates against Ebola Makona Virus. *Nature* **2015**, *520* (7549), 688–691.

(19) Wolfe, D. N.; Zarrabian, A. G.; Disbrow, G. L.; Espeland, E. M. Progress towards a Vaccine against Ebola to Meet Emergency Medical Countermeasure Needs. *Vaccine* **2017**.

(20) Qiu, X.; Wong, G.; Audet, J.; Bello, A.; Fernando, L.; Alimonti, J. B.; Fausther-Bovendo, H.; Wei, H.; Aviles, J.; Hiatt, E.; et al. Reversion of Advanced Ebola Virus Disease in Nonhuman Primates with ZMapp. *Nature* **2014**, *514* (7520), 47–53.

(21) Warren, T. K.; Jordan, R.; Lo, M. K.; Ray, A. S.; Mackman, R. L.; Soloveva, V.; Siegel, D.; Perron, M.; Bannister, R.; Hui, H. C.; et al. Therapeutic Efficacy of the Small Molecule GS-5734 against Ebola Virus in Rhesus Monkeys. *Nature* **2016**, *531* (7594), nature17180.

(22) Sanchez, A. Analysis of Filovirus Entry into Vero E6 Cells, Using Inhibitors of Endocytosis, Endosomal Acidification, Structural Integrity, and Cathepsin (B and L) Activity. *J. Infect. Dis.* **2007**, *196 Suppl 2*, S251-258.

(23) Müller, K. H.; Kainov, D. E.; El Bakkouri, K.; Saelens, X.; De Brabander, J. K.; Kittel, C.; Samm, E.; Muller, C. P. The Proton Translocation Domain of Cellular Vacuolar ATPase Provides a Target for the Treatment of Influenza A Virus Infections. *Br. J. Pharmacol.* **2011**, *164* (2), 344–357.

(24) Mosso, C.; Galván-Mendoza, I. J.; Ludert, J. E.; del Angel, R. M. Endocytic Pathway Followed by Dengue Virus to Infect the Mosquito Cell Line C6/36 HT. *Virology* **2008**, *378* (1), 193–199.

(25) Hunt, S. R.; Hernandez, R.; Brown, D. T. Role of the Vacuolar-ATPase in Sindbis Virus Infection. *J. Virol.* **2011**, *85* (3), 1257–1266.

(26) Chandran, K.; Sullivan, N. J.; Felbor, U.; Whelan, S. P.; Cunningham, J. M. Endosomal Proteolysis of the Ebola Virus

Glycoprotein Is Necessary for Infection. *Science* **2005**, *308* (5728), 1643–1645.

(27) Cotter, K.; Stransky, L.; McGuire, C.; Forgac, M. Recent Insights into the Structure, Regulation, and Function of the V-ATPases. *Trends Biochem. Sci.* **2015**, *40* (10), 611–622.

(28) Brown, D.; Paunescu, T. G.; Breton, S.; Marshansky, V. Regulation of the V-ATPase in Kidney Epithelial Cells: Dual Role in Acid-Base Homeostasis and Vesicle Trafficking. *J. Exp. Biol.* **2009**, *212* (Pt 11), 1762–1772.

(29) Thomas, L.; Rao, Z.; Gerstmeier, J.; Raasch, M.; Weinigel, C.; Rummler, S.; Menche, D.; Müller, R.; Pergola, C.; Mosig, A.; et al. Selective Upregulation of TNFα Expression in Classically-Activated Human Monocyte-Derived Macrophages (M1) through Pharmacological Interference with V-ATPase. *Biochem. Pharmacol.* **2017**, *130*, 71–82.

(30) Rahman, S.; Yamato, I.; Murata, T. Function and Regulation of Mammalian V-ATPase Isoforms. In *Regulation of Ca2+-ATPases,V-ATPases and F-ATPases*; Advances in Biochemistry in Health and Disease; Springer, Cham, 2016; pp 283–299.

(31) Fordyce, C. A.; Grimes, M. M.; Licon-Munoz, Y.; Chan, C.-Y.; Parra, K. J. Vacuolar ATPase in Physiology and Pathology: Roles in Neurobiology, Infectious Disease, and Cancer. In *Regulation of Ca2+-ATPases,V-ATPases and F-ATPases*; Chakraborti, S., Dhalla, N. S., Eds.; Advances in Biochemistry in Health and Disease; Springer International Publishing, 2016; pp 337–369.

(32) Huss, M.; Wieczorek, H. Inhibitors of V-ATPases: Old and New Players. *J. Exp. Biol.* **2009**, *212* (3), 341–346.

(33) Keeling, D. J.; Herslöf, M.; Ryberg, B.; Sjögren, S.; Sölvell, L. Vacuolar H+-ATPases Targets for Drug Discovery? *Ann. N. Y. Acad. Sci.* **1997**, *834* (1), 600–608.

(34) Sørensen, M. G.; Henriksen, K.; Neutzsky-Wulff, A. V; Dziegiel, M. H.; Karsdal, M. A. Diphyllin, a Novel and Naturally Potent V-ATPase Inhibitor, Abrogates Acidification of the Osteoclastic Resorption Lacunae and Bone Resorption. *J. Bone Miner. Res. Off. J. Am. Soc. Bone Miner. Res.* **2007**, *22* (10), 1640–1648.

(35) Shen, W.; Zou, X.; Chen, M.; Liu, P.; Shen, Y.; Huang, S.; Guo, H.; Zhang, L. Effects of Diphyllin as a Novel V-ATPase Inhibitor on Gastric Adenocarcinoma. *Eur. J. Pharmacol.* **2011**, *667* (1–3), 330–338.

(36) König, R.; Stertz, S.; Zhou, Y.; Inoue, A.; Hoffmann, H.-H.; Bhattacharyya, S.; Alamares, J. G.; Tscherne, D. M.; Ortigoza, M. B.; Liang, Y.; et al. Human Host Factors Required for Influenza Virus Replication. *Nature* **2010**, *463* (7282), 813–817.

(37) Chen, H.-W.; Cheng, J. X.; Liu, M.-T.; King, K.; Peng, J.-Y.; Zhang, X.-Q.; Wang, C.-H.; Shresta, S.; Schooley, R. T.; Liu, Y.-T. Inhibitory and Combinatorial Effect of Diphyllin, a v-ATPase Blocker, on Influenza Viruses. *Antiviral Res.* **2013**, *99* (3), 371–382.

(38) Rivera, A.; Messaoudi, I. Molecular Mechanisms of Ebola Pathogenesis. *J. Leukoc. Biol.* **2016**, *100* (5), 889–904.

(39) Charlton, J. L. Antiviral Activity of Lignans. *J. Nat. Prod.* **1998**, *61* (11), 1447–1451.

(40) Daina, A.; Michielin, O.; Zoete, V. SwissADME: A Free Web Tool to Evaluate Pharmacokinetics, Drug-Likeness and Medicinal Chemistry Friendliness of Small Molecules. *Sci. Rep.* **2017**, *7*, srep42717.

(41) Palmgren, M. G. Acridine Orange as a Probe for Measuring PH Gradients across Membranes: Mechanism and Limitations. *Anal. Biochem.* **1991**, *192* (2), 316–321.

(42) Elshabrawy, H. A.; Fan, J.; Haddad, C. S.; Ratia, K.; Broder, C. C.; Caffrey, M.; Prabhakar, B. S. Identification of a Broad-Spectrum Antiviral Small Molecule against Severe Acute Respiratory Syndrome Coronavirus and Ebola, Hendra, and Nipah Viruses by Using a Novel High-Throughput Screening Assay. *J. Virol.* **2014**, *88* (8), 4353–4365.

(43) Basu, A.; Li, B.; Mills, D. M.; Panchal, R. G.; Cardinale, S. C.; Butler, M. M.; Peet, N. P.; Majgier-Baranowska, H.; Williams, J. D.; Patel, I.; et al. Identification of a Small-Molecule Entry Inhibitor for Filoviruses. *J. Virol.* **2011**, *85* (7), 3106–3119.

(44) Aldrich, L. N.; Kuo, S.-Y.; Castoreno, A. B.; Goel, G.; Kuballa, P.; Rees, M. G.; Seashore-Ludlow, B. A.; Cheah, J. H.; Latorre, I. J.; Schreiber, S. L.; et al. Discovery of a Small-Molecule Probe for V-ATPase Function. *J. Am. Chem. Soc.* **2015**, *137* (16), 5563–5568.

(45) Gnirß, K.; Kühl, A.; Karsten, C.; Glowacka, I.; Bertram, S.; Kaup, F.; Hofmann, H.; Pöhlmann, S. Cathepsins B and L Activate Ebola but Not Marburg Virus Glycoproteins for Efficient Entry into Cell Lines and Macrophages Independent of TMPRSS2 Expression. *Virology* **2012**, *424* (1), 3–10.

(46) Charlton, J. L.; Oleschuk, C. J.; Chee, G.-L. Hindered Rotation in Arylnaphthalene Lignans. *J. Org. Chem.* **1996**, *61* (10), 3452–3457.

(47) Zoncu, R.; Bar-Peled, L.; Efeyan, A.; Wang, S.; Sancak, Y.; Sabatini, D. M. MTORC1 Senses Lysosomal Amino Acids Through an Inside-Out Mechanism That Requires the Vacuolar H+-ATPase. *Science* **2011**, *334* (6056), 678–683.

…

Entry for the Table of Contents

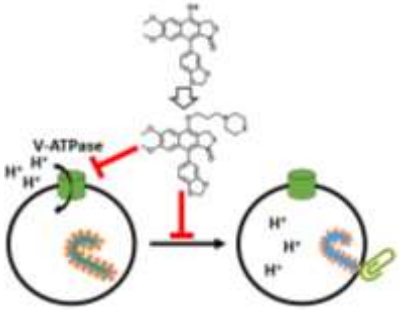

Novel Ebolavirus therapies: Vacuolar-ATPase inhibitors were created and identified as therapeutically-selective inhibitors of Ebolavirus infection. Four series of derivatives of the natural product diphyllin were screened for activity against Ebolavirus infection and cellular V-ATPase activity. Phenol alkylation was identified as a potent method for increasing derivative activity and several alkylamino phenol derivatives exhibited therapeutic selectivity greater than any previous V-ATPase inhibitor.